

Evidence from Tm anomalies for non-CI refractory lithophile element proportions in terrestrial planets and achondrites

Barrat Jean-Alix ^{1,*}, Dauphas N. ², Gillet P. ³, Bollinger C. ⁴, Etoubleau Joel ⁵, Bischoff A. ⁶, Yamaguchi A. ⁷

¹ Université de Bretagne Occidentale, Institut Universitaire Européen de la Mer, CNRS UMR 6538, Place Nicolas Copernic, 29280 Plouzané, France

² Origins Laboratory, Department of the Geophysical Sciences and Enrico Fermi Institute, The University of Chicago, 5734 South Ellis Avenue, Chicago, IL 60637, USA

³ Ecole Polytechnique Fédérale de Lausanne (EPFL), Institute of Condensed Matter Physics, Station 3, CH-1015 Lausanne, Switzerland

⁴ Institut Universitaire Européen de la Mer, CNRS UMS 3113, Place Nicolas Copernic, 29280 Plouzané Cedex, France

⁵ IFREMER, Centre de Brest, 29280 Plouzané, France

⁶ Institut für Planetologie, Westfälische Wilhelms-Universität Münster, Wilhelm-Klemm-Str. 10, 48149 Münster, Germany

⁷ National Institute of Polar Research, Tachikawa, Tokyo 190-8518, Japan and Department of Polar Science, School of Multidisciplinary Science, SOKENDAI (The Graduate University for Advanced Studies), Tachikawa, Tokyo 190-8518, Japan

* Corresponding author : Jean-Alix Barrat, email address : barrat@univ-brest.fr

Abstract :

Thulium is a heavy rare earth element (REE) whose geochemical behavior is intermediate between Er and Yb, and that is not expected to be decoupled from these elements during accretion of planetary bodies and geological processes. However, irregularities in REE volatilities at higher temperature could have decoupled the REEs relative to one another during the early stages of condensation of the solar nebula. Indeed, positive Tm anomalies are found in some refractory inclusions from carbonaceous chondrites, and it is possible that large scale nebular reservoirs displaying positive or negative Tm anomalies were formed during the early history of the solar system. We analyzed a series of meteorites and terrestrial rocks in order to evaluate the existence of Tm anomalies in planetary materials. Relative to CIs (Ivuna-type carbonaceous chondrites), carbonaceous chondrites display unresolved or positive Tm anomalies, while most of the noncarbonaceous chondrites show slightly negative Tm anomalies. Quantification of these anomalies in terrestrial samples is complicated when samples display fractionated heavy REE patterns. Taking this effect into account, we show that the Earth, Mars, Vesta, the aubrite and ureilite parent bodies display small negative anomalies ($Tm/Tm^* \approx 0.975$), very similar to those found in ordinary and enstatite chondrites. We suggest that a slight negative Tm anomaly relative to CI is a widespread feature of the materials from the inner solar system. This finding suggests that CI chondrites may not be appropriate for normalizing REE abundance patterns of most planetary materials as they may be enriched in a high-temperature refractory component with non-solar composition. The presence of Tm anomalies at a bulk planetary scale is, to this day, the strongest piece of evidence that

refractory lithophile elements are not present in constant proportions in planetary bodies.

Keywords : Rare Earth Elements (REE), Achondrite, Earth, Mars, Tm anomaly

1. Introduction

Rare Earth Elements (REEs) are a group of elements whose geochemical properties are very similar to each other. They are generally trivalent with ionic radii decreasing smoothly from La to Lu. The coherence of their behaviors makes them prime elements for geochemical modeling. Their abundances are classically shown with “Masuda-Coryell plots”, where the ratio of each REE concentration to the corresponding value in a reference is plotted as a function of atomic number (Masuda, 1962; Coryell et al., 1963). The references most commonly used in this normalization scheme are a CI chondrite average (e.g., Anders and Grevesse, 1989; Pourmand et al., 2012; Barrat et al., 2012; Palme et al., 2014) and post Archean Australian shale (PAAS; e.g., Nance and Taylor, 1976; Taylor and McLennan, 1985; Pourmand et al., 2012). The resulting curves, known as REE patterns, became one of the most widely used tools to trace geological processes (e.g., Frey et al., 1978; Hanson, 1980; Taylor and McLennan, 1981). These diagrams provide a means of assessing the REE abundances of many samples at a glance, and to detect easily the decoupling of some elements relative

to their neighbors, when the conditions that prevail in the system compel them to a different valence. On Earth for example, Eu and Ce anomalies are found in many magmatic rocks and in aqueous surface environments, respectively when Eu and Ce are present in their 2+ or 4+ valence states while other lanthanides are in their 3+ valence state.

REEs are refractory elements, meaning that their temperatures of condensation during cooling of a solar gas composition at conditions relevant to the formation of the solar system are higher than those of major elements such as Mg or Si (e.g., Boynton, 1975; Davis and Grossman, 1979; Lodders, 2003). Their temperatures of condensation vary from one REE to another, so they can be fractionated from each other at high temperature during evaporation or condensation processes (e.g., Pack et al., 2004 and references therein). This is best illustrated with refractory inclusions found in chondrites, which are the first solids formed in the solar system, that display distinctive volatility-controlled REE patterns with a variety of Ce, Sm, Eu, Tm and Yb anomalies (e.g., Tanaka and Masuda, 1973; Mason and Taylor, 1982; MacPherson, 2003; Fegley and Ireland, 1991; Hiyagon et al., 2011 and references therein).

Inductively Coupled Plasma-Mass Spectrometry (ICP-MS) is established as a premier technique for the determination of trace element abundances in rocks. Unlike previous analytical procedures such as neutron activation or isotope dilution-thermo-ionization mass spectrometry, ICP-MS can simultaneously measure the concentrations of all the REEs present in a given sample. Thus, ICP-MS can allow us to detect small anomalies that were previously not accessible using earlier techniques.

Until recently, it was thought that the REE patterns of terrestrial rocks could only display Eu or Ce anomalies. Thus, the discovery of slight negative Tm anomalies in shales when normalized to CI chondrite was surprising (Pourmand et al., 2012). This observation was subsequently confirmed in some other terrestrial samples and extended to ordinary chondrites, enstatite chondrites, samples from Mars, Moon and Vesta (Bendel et al. 2011, 2012a,b; Dauphas and Pourmand, 2015). Because the negative Tm anomalies obtained in planetary materials by previous workers are small (a few percent), one may argue that they could be at the limit of the precision of the analytical methods, or artifacts produced by an overestimation of the Tm abundance in the chondritic reference. In this paper, we report on analyses obtained on 87 terrestrial and meteoritic samples using a well-established ICP-MS procedure (e.g., Barrat et al., 2012). Our aim is firstly to confirm the Tm abundance in average CI chondrites, secondly to evaluate the diversity of Tm anomalies in differentiated planetary bodies such as Mars and Vesta, which were not investigated in the recent study of Dauphas and Pourmand (2015), which focused on chondrites and Earth, and finally to determine the Tm anomaly of the bulk Earth.

2. Samples and analytical methods

Seventeen chondrites, seven eucrites (from asteroid 4 Vesta), six shergottites (from Mars), one lunar meteorite, nine other achondrites (ureilites, aubrites, one angrite and one ungrouped achondrite), forty-six samples from the Earth (including reference materials), and one olivine fraction from a pallasite, were selected in order to capture the diversity of chondrites and magmatic rocks from Earth, Mars and asteroids. These samples were obtained during the last twenty-five years from various sources including the Muséum National d'Histoire Naturelle de Paris (MNHN), Ifremer (Plouzané, France), Université de Rennes 1 (France), Université de Paris VI (France), Université de Bretagne Occidentale (Brest), the National Institute of Polar research (Tokyo), the Natural History Museum, Vienna, the Smithsonian Institution, the Meteorite Working Group (NASA), the Institute for Meteoritics, Albuquerque, the Northern Arizona University, Flagstaff, and meteorite collectors. The details of the meteorite samples used in this study are given in supplementary Table S1.

Most of the samples were previously characterized extensively for their chemical and mineralogical compositions. The concentrations of some REEs were previously determined in various laboratories using different analytical techniques but with a few exceptions, mono-isotopic Tm was not analyzed. In this study, REE abundances were determined using a Thermo Element 2 ICP-mass spectrometer at Institut Universitaire Européen de la Mer (IUEM), Plouzané, following a well-established procedure first developed at the University of Southampton and Université Joseph Fourier (Barrat et al., 1996), and regularly improved since then (e.g., Barrat et al., 2012). The methodology is briefly summarized below.

Samples were finely powdered using a boron carbide mortar and pestle. Typically, 120 mg of the powder were dissolved in closed screw-top teflon vessels (Savillex) at about 130 °C for three days using 5 ml of concentrated HF and 2 ml of concentrated HNO₃. The vessels were then opened. After evaporation to dryness of the acid mixture, approximately 2 ml of HNO₃ was added, and the vessels were capped and put back on the hot plate and left overnight. The samples were then dried again, and taken up in about 20 g of 6 M HCl ("mother solutions"). No residual grains were observed in the mother solutions except for ureilites, which contained some carbon grains (low REE concentration graphite and diamond) having no impact on the results. Only reagents double-distilled in quartz or teflon sub-boilers were used. For each sample, the abundances of REEs were determined using two aliquots of the mother solution.

A first aliquot of the mother solution was dried and the residue was taken up and dissolved in diluted HNO₃ (2 %) containing traces of HF. This sample solution (solution 1) was analyzed in triplicate, in a sequence containing a procedural blank, a BHVO-2 reference solution (prepared like the

samples), and a series of solutions for the corrections of oxide and hydroxide interferences (pure water, Ba+Ce, Pr+Nd, and Sm+Eu+Gd+Tb solution, see Barrat et al. (1996) for more details). One BHVO-2 reference solution was analyzed every three samples and used for both calibration and drift corrections. The raw data were first corrected for drift, procedural blank and interferences. $[X]_1$, the raw concentration of a given element X in sample was calculated using the corrected data for the BHVO-2 and sample solutions. Then, the three analyses obtained for each sample were averaged.

A second aliquot of the mother solution was spiked with a pure solution of Tm, and processed like the previous one. The spiked sample solution (solution 2) was analyzed using a separate sequence similar to that used for unspiked samples. The REE abundances (except Tm) in the sample are calculated with the following equation (Barrat et al., 1996):

$$[X]_2 = (C_x / C'_{Tm1}) (M_{Tm} / M) / [(C_{Tm} / C'_{Tm1}) - 1] \quad (1)$$

Where $[X]_2$ and C_x are the concentrations of the element X in the sample and in the solution 2, respectively. C_{Tm} and C'_{Tm1} are respectively the concentration of Tm in solution 2 and the estimated concentration of Tm in this solution without the contribution of the spike. C'_{Tm1} was directly calculated using the Tm/Er and Tm/Yb ratios previously obtained for the unspiked solution (solution 1). M is the mass of sample contained in the aliquot of the mother solution used to prepare solution 2, and M_{Tm} is the amount of Tm added. Note that the choice of a Tm-spike here is not specific to the present study but corresponds to the routine procedure used by the first author in Brest.

REE abundances obtained with solutions 1 and 2 are of course very similar, but Tm abundances cannot be determined using solution 2. However, the concentrations obtained with solution 2 are considered more robust, because less affected by the errors on the dilution factors, and less prone to the instrumental drift (Barrat et al., 1996) than the concentrations calculated with solution 1. On the other hand, REE ratios determined with the unspiked solution (solution 1) are more accurate because the solution was run in triplicate. Therefore, $[X]$, the final REE concentrations were calculated combining $[X]_1$ and $[X]_2$, the results for both solutions as follow:

$$[X] = K [X]_1 \quad (2)$$

where $K = ([La]_2/[La]_1 + [Ce]_2/[Ce]_1 + [Pr]_2/[Pr]_1 + [Nd]_2/[Nd]_1 + [Sm]_2/[Sm]_1 + [Eu]_2/[Eu]_1 + [Gd]_2/[Gd]_1 + [Tb]_2/[Tb]_1 + [Dy]_2/[Dy]_1 + [Ho]_2/[Ho]_1 + [Er]_2/[Er]_1 + [Yb]_2/[Yb]_1 + [Lu]_2/[Lu]_1) / 13$

Two samples (NWA 7325, and an olivine separate from the Brenham pallasite) display very low heavy REE abundances ($< 0.1 \times CI$). Their REEs were concentrated and separated from the major

elements before analysis following the method described by Barrat et al. (1996). These two samples were previously analyzed without REE separation and Tm abundances were not available (Greenwood et al., 2015; Barrat et al., 2015). The new analyses now include Tm, and the other REE abundances are in excellent agreement with the previous ones (the previous and new analyses usually agree within 4%).

The results for international reference materials are given in Table 1, relative to our working values for the USGS basalt BHVO-2. The latter were derived from the isotope dilution results obtained by Raczek et al. (2001) for La, Ce, Nd, Sm, Eu, Gd, Dy, Er, Yb and Lu, and from our previous ICP-MS analyses for Pr, Tb, Ho, and Tm (Barrat et al., 2012). In the event of future change to these BHVO-2 values, the data need only to be corrected by the ratio of the new and old values. Based on replicate analyses of standard reference materials and samples (Barrat et al., 2012, 2014), the precision for REE abundances is much better than 3 % (one relative standard deviation - RSD).

The accuracy of our results is of course directly linked to the accuracy of our working values for BHVO-2. At present, BHVO-2 is one of the best characterized reference materials for REEs, and our working values are very similar to the GEOREM's preferred values (georem.mpch-mainz.gwdg.de). Furthermore, the results obtained for other well-characterized reference materials (e.g., Bayon et al., 2009; Barrat et al., 2012, 2014) confirm that the BHVO-2 working values are accurate and validate our calibration, as exemplified here by the results obtained for BIR-1 and BCR-2 (Table 1 and Fig. 2), which are other well-known reference materials.

The Tm anomalies can be estimated using the Tm/Tm^* ratio, where Tm^* is the interpolated Tm concentration for a smooth CI-normalized REE pattern and X_n is the concentration of element X normalized to chondrite:

$$Tm/Tm^* = (Tm_n) / (Er_n \times Yb_n)^{1/2} \quad (3)$$

The relative standard deviations of Tm/Tm^* values based on replicate BCR-2 and BIR-1 are better than 0.6 % and 0.3 %, respectively (Table 1). From the results obtained for both reference materials and sample replicates, we estimate that the precision of Tm/Tm^* measurements is better than 0.7 % (1 RSD).

Dauphas and Pourmand (2015) used different equations to estimate the Tm anomalies. In a first equation, Tm^* is interpolated linearly using the logarithm of the CI-normalized abundances against ionic radius of Er and Yb:

$$(Tm/Tm^*)_{D\&P} = (Tm_n) / (Er_n^{0.55} \times Yb_n^{0.45}) \quad (4)$$

As shown in Figure 1, the Tm anomalies obtained using this equation are similar to those obtained with equation (3). Moreover, Dauphas and Pourmand (2015) proposed a second estimation of the Tm anomalies using Er and Lu, because Yb can be decoupled from the other REEs in highly reducing conditions (e.g., Pack et al., 2004):

$$(Tm/Tm^{**})_{D\&P} = (Tm_n) / (Er_n^{0.66} \times Lu_n^{0.34}) \quad (5)$$

Finally, they noticed that the curvature of the REE patterns could affect the Tm anomalies when based on simple linear interpolations. They proposed a third approach for normalizing Tm by using a Lagrangian (3rd order polynomial) interpolation between four REEs, Dy, Ho, Er and Lu:

$$(Tm/Tm^{***})_{D\&P} = (Tm_n) / (Dy_n^{0.33} \times Ho_n^{-1.29} \times Er_n^{1.85} \times Lu_n^{0.11}) \quad (6)$$

The enstatite meteorites that we have analyzed do not display negative Yb anomalies. The $(Tm/Tm^*)_{D\&P}$ and Tm/Tm^* ratios are very similar (Fig. 1), and consequently the use of equation 5 is not necessary to compare our enstatite chondrites (EC) samples with the other chondrites. Although the $(Tm/Tm^{**})_{D\&P}$ and $(Tm/Tm^{***})_{D\&P}$ ratios have their advantages, they will not be used here. In the rest of the paper, we will use the Tm/Tm^* ratios calculated using equation 3 because these ratios provide a precise estimate of the Tm-anomalies, are coherent with the inter-element distance in usual REE plots, and provide in most cases, the same information as the $(Tm/Tm^*)_{D\&P}$ and $(Tm/Tm^{***})_{D\&P}$ ratios. In order to better discuss the curvature effect (CE) of the REE pattern, an additional equation is preferred. We use a Lagrangian interpolation like Dauphas and Pourmand (2015), but with two elements at each side of Tm (Ho, Er, Yb, Lu):

$$Tm/Tm^*_{CE} = Tm_n / [(Yb_n \times Er_n)^4 / (Lu_n \times Ho_n)]^{1/6} \quad (7)$$

As shown in Figure 1, the Tm/Tm^*_{CE} ratios are more strongly correlated with Tm/Tm^* than the $(Tm/Tm^{***})_{D\&P}$ ratios, suggesting that the effect of the shape of the REE pattern is more correctly taken into account with equation 7. The effect of the curvature of the pattern on the calculated Tm/Tm^* ratio for each sample can be discussed using the CE# number, defined here as the Tm^*_{CE} / Tm^* ratio:

$$CE\# = Tm^*_{CE} / Tm^* = [(Yb_n \times Er_n) / (Lu_n \times Ho_n)]^{1/6} \quad (8)$$

If $CE\# \approx 1$ (i.e., in the range 0.99-1.01), the curvature effect is negligible, and the Tm anomaly estimated using equation 3 is reliable. If $CE\# < 1$, the Tm/Tm^* ratio amplifies the negative Tm anomalies and reduces the positive ones. If $CE\# > 1$, the opposite effects are obtained. As we will see for terrestrial lavas, the shapes of the REE patterns can have a significant effect on the Tm/Tm^* ratios. Although, these shapes do not generate anomalous or aberrant Tm anomalies, the curvature effects must be taken into account when the Tm/Tm^* ratios of samples with very different REE patterns are compared.

The choice of the normalizing values (i.e., CI concentrations) has an important impact on the values of the calculated Tm/Tm^* ratios. However, it has no effect on the offsets between samples of various types. Here we have adopted the CI average recommended by Barrat et al. (2012) because this average was obtained from five “large” samples prepared from distinct stones of Orgueil, which comprise ca. 4 g of this meteorite. *More importantly, the Orgueil analyses were obtained using the same procedure and the same calibration strategy as the analyses presented here, minimizing any possible systematic bias.* We have reanalyzed aliquots of our Orgueil samples (see below), and the new results confirm the results from Barrat et al. (2012), so that revision of the normalizing values is not necessary.

The Tm anomalies reported in this study are small ($< 15\%$), but significant as illustrated by the reference materials (Table 1): BIR-1 ($Tm/Tm^*=0.978$, $1\sigma = 0.003$, Table 1) and BCR-2 ($Tm/Tm^*= 0.970$, $1\sigma = 0.006$, Table 1) have Tm/Tm^* ratios that are respectively 7σ and 5σ below the mean CI value. Comparison with literature results is not straightforward because systematic biases between laboratories are present (Fig. 2). To mitigate this problem, we have adjusted the results obtained by Pourmand et al. (2012, 2014), Stracke et al. (2012), Dauphas and Pourmand (2015) to our calibration using BIR-1, BCR-2, and BHVO-2, and Khan et al. (2015) using the Smithsonian Institution Allende powder (USNM 3529) as follow:

$$(Tm/Tm^*)_{\text{sample,corrected}} = (Tm/Tm^*)_{\text{standard,Brest}} \times (Tm/Tm^*)_{\text{sample,measured}} / (Tm/Tm^*)_{\text{standard,measured}} \quad (9)$$

where Tm^* is calculated using the average CI abundances obtained by Barrat et al. (2012), and (standard refers to BHVO-2, BIR-1, BCR-2 or USNM 3529 depending on the study considered). When the literature data were accompanied by two or more standards, the corrected Tm/Tm^* ratios were averaged. The corrections were small and similar when two or more standards were considered: about 3% for the data obtained by Dauphas and Pourmand (2015) and about 2% for the data obtained by Stracke et al. (2012). All values reported or discussed in this paper are relative to our BHVO-2 working values.

3. Results

Results are given in Tables 1 to 4. The REE abundances of the meteorites and terrestrial rocks analyzed here, are discussed extensively in the literature, and in depth discussions concerning the shape of the REE patterns will not be repeated here. Instead, our study is focused on Tm anomalies, which are small and not always discernable in the REE patterns, as demonstrated in Figure 3. The Tm/Tm* ratios are presented in Figure 4 along with selected literature data. A synthesis of the Tm/Tm* ratios in meteorites and bulk planetary bodies is given in Table 5.

3.1 *Tm abundance in the CI reference*

Large chips of Orgueil and Ivuna were previously analyzed, and the average of five Orgueil samples was recommended for normalization purposes (Barrat et al., 2012). In order to check the normalization values for the heavy REEs, we dissolved 30 mg splits of the previous CI powders (previous analyses of the same samples were obtained using about 120-150 mg of powders). The results display a limited range of Tm/Tm* ratios from 0.991 to 1.003 (Table 2), with a mean = 0.999 ($\sigma=0.005$, $n=10$). These results indicate that our CI average used for normalization does not require revision at the present level of precision. Pourmand et al. (2012) obtained Tm/Tm* ratios ranging from 0.999 to 1.043, and consequently a CI average with a small positive anomaly relative to our results (Tm/Tm*=1.022 after correction of the interlaboratory bias). This small discrepancy could be at least partially explained by the small size of most of the chips analyzed by these authors, totaling ca. 2.14 g for Orgueil, Alais and Ivuna, since it is well known that CI chondrites are heavily brecciated and chemically heterogeneous at the sub-mm scale (e.g., Morlok et al., 2006). It is also conceivable that CIs contain rare refractory inclusions (or their remnants after aqueous alteration) which could have affected their Tm abundances (Bendel et al., 2012a,b). Although one small CAI was found in Ivuna (Frank et al., 2011), the limited range of Tm/Tm* ratios shown by our samples is not consistent with the occurrence of heterogeneously dispersed refractory inclusions.

3.2 *Tm anomalies in other chondrites*

The abundance of Tm in chondrites has been measured in a large number of samples by Bendel et al. (2011, 2012a, b), Stracke et al. (2012), Khan et al. (2015), Pourmand et al. (2012) and Dauphas and Pourmand (2015). CM chondrites (Paris, Nogoya and Boriskino), enstatite chondrites (3 EH and 3 EL) and ordinary chondrites (Chelyabinsk and Braunschweig) have been analyzed here (Fig. 4 and Tables 2-3). Because all these chondrites have CE#-numbers very close to 1 (=0.995-1.006, Table 2), their Tm/Tm* ratios are unaffected by curvature in REE patterns and are faithful measures of Tm anomalies. The three CM samples display Tm/Tm*>1 (i.e., from 1.009 to 1.036) contrary to the two ordinary (average Tm/Tm*= 0.972, $n=2$) and the six enstatite chondrites (average Tm/Tm*=

0.983, $\sigma = 0.003$, $n=6$) which all show small negative Tm anomalies. For all these types of chondrites, the new results are in good agreement with data obtained by Dauphas and Pourmand (2015). However, our results for enstatite chondrites appear much more homogeneous than the previously published data (Fig. 4 and Table 5).

3.3 *Tm anomalies in achondrites and pallasite*

Except for the Brenham olivine and NWA 7325, all our achondrite samples have CE#-numbers very close to one ($=0.991-1.003$, Table 3), indicating again that their Tm/Tm* ratios are faithful measures of Tm anomalies. The Tm/Tm* ratios measured on seven eucrites (four main group - Nuevo Laredo trend eucrites: Bereba, Juvinas, NWA 049 and Nuevo Laredo; three Stannern trend eucrites: Stannern, Bouvante, and NWA 2061) are very homogeneous, and range from 0.972 to 0.978. Their average Tm/Tm* ratio ($= 0.974$, $\sigma = 0.002$) is similar to the average of ordinary chondrites ($=0.977$, $\sigma = 0.006$, $n=22$, see Table 5).

Similar negative Tm anomalies were obtained for the angrite NWA 1296, and for five aubrites including the samples analyzed by Dauphas and Pourmand (2015). Moreover, the four ureilites analyzed here display analogous negative Tm anomalies (Tm/Tm* $=0.964-0.983$), like the value measured previously for an Almahata Sitta trachyandesite (Tm/Tm* $=0.972$) from the same parent-body (Bischoff et al., 2014). These results strengthen the “noncarbonaceous pedigree” of the ureilite parent body despite the high C contents of the ureilites, as previously suggested by Yamakawa et al. (2010) and Warren (2011a) from isotopic anomalies.

The REE pattern of the Brenham olivine is enriched in light REEs, with a slightly convex heavy REE distribution (see Fig. 7 in Greenwood et al., 2015). Indeed, the CE#-number is low ($=0.976$) and the curvature of the pattern cannot be ignored. Although its Tm/Tm* ratio ($=0.975$) is similar to those of other achondrites, the Tm/Tm*_{CE} ratio is 0.999 indicating that no Tm anomaly is present in this pallasite. Other pallasites samples are necessary to determine the Tm/Tm* ratio of the main-group and Eagle Station pallasite parent bodies.

NWA 7325 is an ungrouped achondrite, and it is the sole sample available on Earth from its parent body. It was suggested to have originated from Mercury (Irving et al., 2013), but it is too old to be a sample from the surface of this planet (4562.5 ± 4.4 Ma, Amelin et al., 2013; 4562.8 ± 0.3 Ma, Dunlap et al., 2014). It formed from an unusual melt characterized by very low REE abundances and a very large positive Eu anomaly, generated by the remelting of an ancient gabbroic lithology. NWA 7325 is a remnant of one of the earliest crusts formed on a differentiated body recognized at present (Barrat et al., 2015). It displays the largest negative Tm anomaly analyzed so far in a magmatic rock (Fig. 3). Its

Tm/Tm* ratio (=0.855) is too distinct to be explained solely by a curvature effect of the REE pattern despite a low CE#-number (=0.983). Indeed, its Tm/Tm*_{CE} ratio is similarly low (=0.868). A possible explanation for this low value could be an analytical artifact. NWA 7325 displays a huge positive Eu anomaly, and consequently is characterized by a high Eu/Tm ratio of 313. In the case of Eu-rich rocks, the determination of Tm abundances could possibly be hampered by a ¹⁵³Eu¹⁶O interference on the ¹⁶⁹Tm peak, but the former is generally insignificant. This interference is monitored and corrected for in our procedure (*e.g.*, Barrat et al., 1996). A negative Tm anomaly could be obtained if the Eu oxide interference was overcorrected. We have spiked a sample of BIR-1 with a solution of pure Eu, in order to check this effect. Although the Eu/Tm ratio of the spiked BIR-1 sample (Eu/Tm = 205 instead of 2 in an unspiked sample) is very high, its Tm/Tm* ratio is identical to the results obtained for unspiked samples (Table 1). We conclude that the low Tm/Tm* ratio obtained for NWA 7325 is real.

3.4 *Tm anomalies in Martian meteorites*

Six shergottites selected for this study range in composition from strongly light-REE depleted (Tissint and Dar al Gani 476) to enriched types (NWA 1669 and Los Angeles), including NWA 1950, one of the rare lherzolithic shergottites (Gillet et al., 2005). Their CE# numbers range between 0.992 and 0.997, and indicate that the effects of the curvature of the patterns are insignificant. Indeed, the Tm/Tm* ratios fall within a restricted range from 0.974 to 0.983 (average Tm/Tm* = 0.977, σ = 0.003), nearly identical to the eucrite and ordinary chondrite values.

3.5 *Tm anomalies in terrestrial and lunar rocks*

Three types of samples were selected: recent lavas (n=42 including reference materials), mainly basalts, from all the oceans and from different geological settings (mid ocean ridge basalts, ocean island basalts, continental alkali basalts, island arc lavas), tektites (two indochinites and two Libyan Desert glasses) formed from the melting of sedimentary protoliths (*e.g.*, Koeberl, 1992, Barrat et al., 1997), and a lunar meteorite.

Terrestrial lavas display a wide range of compositions, with a large diversity of REE patterns. Our sampling encompasses a large variety of lavas ranging from light-REE depleted oceanic basalts with no important curvature for the heavy REEs to alkali lavas with strongly fractionated patterns (*e.g.*, lavas from Tubuai or from the French Massif Central). The curvature of the REE patterns is significant for some samples: the CE#-numbers of the lavas range from 0.978 to 0.999. All lavas display a slight negative Tm anomaly and the Tm/Tm* ratios show a significant range of variability, from 0.946 to 0.988 (Fig. 4). The mean Tm/Tm* ratio (=0.965, σ =0.011, n=42) for all lavas including the reference materials BE-N, BIR-1, BHVO-2, JA3, and JB2, is slightly lower than the Vestan and Martian means. The spread of the Tm/Tm* ratios is chiefly explained by a curvature effect of the REE

patterns. Indeed, the samples with the lowest CE#-numbers exhibit among the lowest Tm/Tm^* ratios (Fig. 5). A more limited range of values is obtained if Tm/Tm^*_{CE} ratios are considered (Fig. 5).

Although the number of high quality Tm analyses of upper crustal rocks available at present is limited, their Tm/Tm^* ratios overlap and extend the range obtained for basaltic lavas to lower values (Fig. 4). The REE patterns of the two indochinites are nearly identical, with slight negative Tm anomalies (0.975-0.981) similar to those observed in shales (Figures 4 and 6). A Tm/Tm^* as low as 0.933 was measured by Dauphas and Pourmand (2015) for G3 granite, a reference material. These authors interpreted the scatter in Tm/Tm^* anomalies among terrestrial rocks to reflect the curvature of REE patterns and G3 is indeed a sample that displays a strong curvature ($CE\# = 0.981$). The two Libyan Desert glasses show parallel REE patterns but with slightly more pronounced negative Tm anomalies than shales ($Tm/Tm^* = 0.947-0.954$), and these may not totally explained by the curvature of the patterns (Fig. 6). Volatilization of Tm during impact is a possible explanation. However, Libyan Desert glasses display unfractionated isotope compositions of Zn and Cu in comparison to the terrestrial crust (Moynier et al., 2009, 2010). Because these elements are much more volatile than Tm, preferential volatilization of Tm during impact melting is unlikely. More high quality Tm measurements for upper crustal rocks (including granites and sediments), are necessary to evaluate a possible decoupling of Tm during geological processes.

Dhofar 460, a lunar feldspathic granulitic breccia paired with Dhofar 026, displays a small negative Tm anomaly ($Tm/Tm^* = 0.969$), within error of the terrestrial lava mean.

4. Discussion

4.1 *Origin of the Tm/Tm^* anomalies in chondrites*

The dichotomy of Tm anomalies between carbonaceous and non-carbonaceous chondrites is confirmed by our new analyses. All carbonaceous chondrites analyzed so far display unresolved to positive Tm anomalies relative to CI, while most of the non-carbonaceous chondrites exhibit negative Tm anomalies. These negative anomalies are subtle, on the order of just a couple of percent (Tm/Tm^* typically close to 0.975), and less marked than those calculated by Dauphas and Pourmand (2015) (Tm/Tm^* typically close to 0.96), due to the different CI averages used for normalization.

Large positive Tm anomalies in some carbonaceous chondrites are well known since a long time, notably in Allende for which they have been interpreted as fingerprints of the presence of group II CAIs (Fig. 6, e.g., Mason and Taylor, 1982; Shinotsuka et al., 1995; Stracke et al., 2012). Thus, it can be inferred that the range of Tm/Tm^* ratios in chondrites is mostly controlled by the distribution

of refractory inclusions or other refractory components. Indeed, Dauphas and Pourmand (2015) pointed out that there is a relationship between Tm anomalies and Ca isotopic fractionation in bulk meteorites. The reason is that CAIs with type II REE patterns also have fractionated Ca isotopic compositions (Huang et al., 2012). Ordinary and enstatite chondrites have slight negative Tm anomalies and $\delta^{44}\text{Ca}$ values close to the terrestrial composition, while carbonaceous chondrites have positive Tm anomalies and heavy $\delta^{44}\text{Ca}$ values relative to Earth. The data plot on mixing trends defined by type II CAIs and by the terrestrial composition as endmembers (Fig. 7). This general pattern is confirmed by the present study but in order to make progress on this topic, one would need to measure Ca isotopes and Tm anomalies in the same aliquots, as carbonaceous chondrites are likely to be heterogeneous at the sampling scale. Some of the carbonaceous chondrites with high Tm/Tm* values relative to inner solar system bodies are devoid of CAIs (e.g., CIs). The carriers of Tm anomalies need not be in the form of grains that aggregated to form CAIs, however. They could also be in the form of disseminated refractory dust grains that carry the same chemical signature but were obliterated by parent-body processes such as aqueous alteration on the CI parent-body. This means that a simple correlation between the modal abundance of CAIs and Tm anomalies is neither expected nor observed.

4.2 *Tm/Tm* ratios of the bulk achondrite parent bodies, Mars and Earth*

Because melting and fractional crystallization most likely do not fractionate Tm abundances from those of Er and Yb, the Tm/Tm* ratios of magmatic rocks or mantle restites from a given planetary body provide a picture of the heterogeneity of the body for this parameter. The restricted ranges of Tm/Tm* ratios exhibited by aubrites, ureilites, eucrites and shergottites indicate that their parent bodies accreted from homogeneous building blocks, or were efficiently homogenized by differentiation processes. Consequently, their mean Tm/Tm* ratios are certainly very good estimates of the Tm/Tm* of their parent bodies (Table 5).

The determination of the Tm anomaly of the bulk Earth is not as straightforward as for those of other telluric bodies, because terrestrial rocks, including lavas and continental rocks, display a puzzling range of Tm/Tm* ratios, from 0.93 to 0.99, which is chiefly explained by the diversity and curvature of their REE patterns (also see Dauphas and Pourmand, 2015). The mean Tm/Tm* ratios of all lavas cannot provide a correct estimate for the bulk Earth because this mean is certainly biased by the alkali lavas, which display the lowest CE#-numbers and Tm/Tm* ratios, and comprise about half of our database. Instead, we estimate the Tm/Tm* ratio of the bulk Earth using only lava samples for which the curvature effect is negligible, in other words those samples with CE# numbers in the range 0.99-1.00. Thus, the Tm/Tm* ratio of our planet is certainly very close to 0.976 (Table 5). This ratio is similar to the mean of the shales (Tm/Tm*=0.974, Table 5) whose CE# numbers are all in the range

0.996-1.003 (Fig. 5). The mean of the shales certainly mirrors the upper continental crust value, and suggests that Tm was not decoupled from other heavy REEs during the formation of the continental crust or sedimentary processes. The lower Tm/Tm* ratio (= 0.963, n=25) displayed by the mean of the aeolian dust analyzed by Pourmand et al. (2014) is not explained at present (Fig. 5), but a slight analytical bias cannot be excluded (Fig. 5).

4.3 Tm/Tm* ratios and non-CI refractory lithophile element abundances

An important observation that emerges from our work is that the Tm/Tm* ratios of the Earth, Mars, Vesta, the UPB, and the aubrite parent body are indistinguishable and close to 0.975 (Fig. 4 and Table 5). This may be a characteristic signature of inner solar system solids (Dauphas and Pourmand, 2015). This inference is strengthened by the results obtained on one angrite, and on ordinary and enstatite chondrites, which all display similar Tm/Tm* ratios as Earth, Mars, and Vesta. The unique achondrite NWA 7325, which crystallized from an impact melt, is the sole sample with a much lower Tm/Tm* ratio. Its parent body could have formed from a minor reservoir with distinctly lower negative Tm anomalies.

The homogeneity of the Tm/Tm* ratios in the bulk Earth, Mars and other small differentiated bodies has important implications. Tm/Tm* ratios are very sensitive to the proportions of group II CAIs in primary materials. Using the mean of the group II CAIs analyzed by Huang et al. (2012) and CI abundances, calculations indicate that Tm/Tm* ratios ranging from 0.97 to 0.98 can be explained by variations in the proportion of Group II CAI-like dust in the order of ± 0.035 wt% only. Thus the materials that formed the Earth and Mars, and much smaller differentiated bodies like Vesta or the aubrite parent body, were extremely homogeneous with respect to heavy REE fractionation, despite a strong heterogeneity in terms of volatile depletions (Fig. 8).

Refractory lithophile elements (RLEs; Ca, Al, Ti, REEs) are usually assumed to be in CI-like proportions in planetary materials, reflecting the fact that they cannot easily be fractionated at a bulk planetary scale by nebular processes. This assumption is very difficult to put to the test because these elements can be fractionated by magmatic and aqueous processes that overprint earlier signatures. The first line of evidence that the Earth may have non-chondritic RLE ratios came from high precision ^{142}Nd isotope measurements which revealed that the accessible Earth may have a Sm/Nd ratio higher than chondritic (Boyet and Carlson, 2005). Nebular processes cannot readily explain this fractionation and it was suggested that either a hidden early formed enriched reservoir with a low Sm/Nd is present in the deep Earth (i.e., a recycled protocrust; Boyet and Carlson, 2005) or a protocrust with low Sm/Nd was lost to space by impact erosion (Caro et al. 2008). Either way, the Earth would have started with a chondritic Sm/Nd ratio. Interpretation of ^{142}Nd is still a matter of contention as subsequent measurements showed that ^{142}Nd variations could be partly explained by the

presence of nucleosynthetic anomalies (Gannoun et al., 2011), so that the silicate Earth may still have chondritic Sm/Nd ratio. The finding of Tm anomalies in bulk planetary materials relative to CIs (this study; Dauphas and Pourmand 2015) demonstrates that the assumption that RLEs are present in CI proportions in Earth and other terrestrial planets is not valid. CIs are enriched in a highly refractory dust component with fractionated RLE abundances relative to inner solar system objects.

Finally, the contribution of carbonaceous chondrites during the main stages of the accretion of the terrestrial planets has been a matter of debates. Many models have been put forward ranging from the involvement of essentially non-carbonaceous chondrites for the Earth and Mars to various proportions of carbonaceous and non-carbonaceous chondrites for the Earth, Mars and Vesta (Sanloup et al., 1999; Lodders, 2000; Burbine and O'Brien, 2004; Warren, 2011b; Javoy et al., 2010; Toplis et al., 2013; Siebert et al., 2013; Dauphas et al., 2014 and references therein). In principle, the Tm anomalies in extraterrestrial materials could offer new constraints for estimates of the proportions of carbonaceous chondrites in terrestrial bodies. Unfortunately the Tm/Tm^* ratio is not very sensitive to the contributions of such material: for example a 75% ordinary chondrite + 25% CM mixture [calculated with Chelyabinsk ($Tm/Tm^*=0.975$) and Paris ($Tm/Tm^*=1.009$)] displays a $Tm/Tm^*=0.983$ just slightly higher than the mean ordinary chondrite value, at the limit of the present level of precision. However, the homogeneity of the Tm/Tm^* ratios for the Earth, Mars and Vesta strongly suggests that carbonaceous chondrites were not the main planetary building materials in the Inner Solar System, in agreement with the systematics of O, Ca, Ti, Cr, and Ni isotopes (e.g., Warren, 2011b; Dauphas et al., 2014).

5. Conclusions

Our analyses of chondrites confirm the dichotomy between carbonaceous and non-carbonaceous chondrites reported by previous studies. Relative to CIs, carbonaceous chondrites display Tm/Tm^* ratios equal to, or higher than one, while the vast majority of the non-carbonaceous chondrites display negative Tm/Tm^* anomalies (Fig. 4). All achondrites and planetary samples analyzed so far display small negative Tm anomalies relative to CIs ($Tm/Tm^*=0.975$), similar to non-carbonaceous chondrites (Fig. 4). Terrestrial rocks show variable Tm/Tm^* ratios that reflect the fact that the use of Er and Yb abundances for normalization to determine Tm anomalies can lead to misleading results if REE patterns display some curvature. Accounting for this curvature effect, we show that the Earth has a Tm/Tm^* ratio of 0.976. One of the most important observations that emerges from our work is that the mean Tm/Tm^* ratios of the Earth, Mars, 4-Vesta, and possibly of most of the parent bodies of achondrites (angrites, ureilites, aubrites) are similar. This suggests that small negative Tm anomalies (typically $Tm/Tm^*=0.975$) were a widespread feature of inner solar system solids. Our data agree with isotope studies, which suggest that carbonaceous chondrites represent a minor fraction of Earth's

building blocks. The presence of negative Tm anomalies in bulk planetary materials (Earth, Mars, Vesta, other achondrite parent bodies) relative to CIs demonstrates that the assumption that refractory lithophile elements are present in CI proportions in planets is unwarranted as CIs are seemingly enriched in a refractory component with a distinct RLE signature.

Acknowledgements

The samples analyzed during the course of this study were kindly provided to the first author during the last 25 years by the Muséum National d'Histoire Naturelle (Paris), Ifremer, the Université Pierre et Marie Curie, the Université de Rennes 1, the Institute for Meteoritics, Albuquerque, the National Institut of Polar Research, Tokyo, the Natural History Museum, Vienna, the Smithsonian Institution, the Meteorite Working Group (NASA), Patrick Bachelery, Ted Bunch, Alain et Louis Carion, Martial Caroff, Bruno and Carine Fectay, Luc Labenne, Robert Roccia, Don Simptson, and our late colleagues Theodore Monod and Jean-Louis Cheminée. US Antarctic meteorite samples are recovered by the Antarctic search for Meteorites (ANSMET) program which has been funded by NSF and NASA, and characterized and curated in the department of Mineral Sciences of the Smithsonian Institution and Astromaterials Curation Office at NASA Johnson Space Center. Special thanks to Frederik Paulsen who kindly provided a large sample of Chelyabinsk. We thank Marc Norman and Mark Rehkämper for the editorial handling and their helpful comments which greatly improved the manuscript, Christine Floss, Herbert Palme, two anonymous reviewers for their constructive comments and Pascale Barrat for her help. This work was supported by the "Laboratoire d'Excellence" LabexMER (ANR-10-LABX-19) and co-funded by grants from the French government under the program "Investissements d'Avenir" and from the Programme National de Planétologie (CNRS-INSU) to the first author.

References

- Amelin Y., Koefoed P., Iizuka T., and Irving A.J. (2013) U-Pb age of ungrouped achondrite NWA 7325. 76th Annual Meteoritical Society Meeting, abstract #5165.
- Anders E. and Grevesse N. (1989) Abundances of the elements: meteoritic and solar. *Geochim. Cosmochim. Acta* **53**, 197–214.
- Barrat J.A., Keller F., Amossé J., Taylor R.N., Nesbitt R.W., Hirata T. (1996) Determination of rare earth elements in sixteen silicate reference samples by ICP-MS after Tm addition and ion exchange separation. *Geostandards Newsletter* **20**, 1, 133-140.
- Barrat J.A., Jahn B.M., Amossé J., Rocchia R., Keller F., Poupeau G.R., Diemer E. (1997). Geochemistry and origin of Libyan Desert glasses. *Geochim. Cosmochim. Acta* **61**, 1953-1959.
- Barrat J.A., Zanda B., Moynier F., Bollinger C., Liorzou C., and Bayon G. (2012) Geochemistry of CI chondrites: Major and trace elements, and Cu and Zn isotopes. *Geochim. Cosmochim. Acta* **83**, 79-92.
- Barrat J.A., Zanda B., Jambon A., Bollinger C. (2014) The lithophile trace elements in enstatite chondrites. *Geochim. Cosmochim. Acta*. **128**, 71-94.
- Barrat J.A., Greenwood R.C., Verchovsky A.B., Gillet Ph., Bollinger C., Liorzou C., Franchi I.A. (2015) Crustal differentiation in the early solar system: clues from the unique achondrite Northwest Africa 7325 (NWA 7325). *Geochim. Cosmochim. Acta*. **168**, 280-292.
- Bayon G., Barrat J.A., Etoubleau J., Benoit M., Révillon S. (2009) Determination of Sc, Y, Zr, Ba, Hf, Th and REE in geological samples by ICP-MS after Tm addition and alkaline fusion. *Geostandards and Geoanalytical Research* **33**, 51-62.
- Bendel V., Patzer A., Pack A., Hezel D.C., Münker C. (2011) Rare Earth Elements in bulk chondrites and chondrites components. 42nd Lunar and Planetary Science Conference, abstract # 1711.
- Bendel V., Pack A., O'Neill H. St. C. (2012a) Rare Earth Elements in CII-chondrites and planetary samples. 43rd Lunar and Planetary Science Conference, abstract # 2578.
- Bendel V., Pack A., O'Neill H. St. C., Jenner F.E., Münker C. (2012b) Volatility-controlled rare earth element fractionation in the early solar system. 75th Annual Meteoritical Society Meeting, abstract # 5351.
- Bischoff A., Horstmann M., Barrat J.A., Chaussidon M., Pack A., Herwartz D., Ward D., Vollmer C., Decker S. (2014) Trachyandesitic volcanism in the early Solar System – constraints from the ureilite parent body. *PNAS* **111**, 35, 12689-12692.
- Boyet M. and Carlson R. W. (2005) ¹⁴²Nd evidence for early (>4.53 Ga) global differentiation of the silicate Earth. *Science* **214**, 427–442.
- Boynton W. V. (1975) Fractionation in the solar nebula: condensation of yttrium and the rare earth elements. *Geochim. Cosmochim. Acta* **39**, 569–584.
- Burbine T.H., O'Brien K.M. (2004) Determining the possible building blocks of the Earth and Mars. *Meteoritics and Planetary Science* **39**, 667-681.
- Caro G., Bourdon B., Halliday A. N. and Quitté G. (2008) Superchondritic Sm/Nd ratios in Mars, the Earth and the Moon. *Nature* **452**, 336–339.
- Coryell C.D., Chase J. W., and Winchester J.W. (1963) A procedure for geochemical interpretation of terrestrial rare-earth abundance patterns. *J. Geophys. Res.* **68**, 559-566.
- Dauphas N., Chen J.H., Zhang J., Papanastassiou D.A., Davis A.M., Travaglio C. (2014) Calcium-48 isotopic anomalies in bulk chondrites and achondrites: evidence for a uniform isotopic reservoir in the inner protoplanetary disk. *Earth and Planetary Science Letters* **407**, 96-108.

Dauphas N, Pourmand A. (2015) Thulium anomalies and rare earth element patterns in meteorites and Earth: Nebular fractionation and the nugget effect. *Geochim. Cosmochim. Acta* **163**, 234-261.

Davis A. M., Grossman L. (1979) Condensation and fractionation of rare earths in the solar nebula. *Geochim. Cosmochim. Acta* **43**, 1611-1632.

Dunlap D. R., Wadhwa M., Romaneillo S. R. (2014) ^{26}Al - ^{26}Mg systematics in the unusual ungrouped achondrite NWA 7325 and the eucrite Juvinas. *45th Lunar Planet. Sci. Conf.*, abstract # 2186.

Fegley B. and Ireland T. R. (1991) Chemistry of the rare earth elements in the solar nebula. *Eur. J. Solid State Inorg. Chem.* **28**, 335-346.

Frank D., Zolensky M., Martinez J., Mikouchi T., Ohsumi K., Hagiya K., Satake W., Le L., Ross D., Peslier A. (2011) A CAI in the Ivuna CII chondrite. *42nd Lunar and Planetary Science Conference*, abstract #2785.

Frey F.A., Green D.H., Roy S.D. (1978) Integrated models of basalt petrogenesis – Study of quartz tholeiites to olivine melilitites from South Eastern Australia utilizing geochemical and experimental petrological data. *J. Petrology* **19**, 463-513.

Gannoun A., Boyet M., Rizo H., El Goresy A. (2011) ^{146}Sm - ^{142}Nd systematics measured in enstatite chondrites reveals a heterogeneous distribution of ^{142}Nd in the solar nebula. *PNAS* **108**, 19, 7693-7697.

Gillet Ph., Barrat J.A., Beck P., Marty B., Greenwood R.C., Franchi I.A., Bohn M., Cotten J. (2005) Petrology, geochemistry, and cosmic-ray exposure age of Northwest Africa 1950. *Meteoritics Planet. Sci.* **40**, 1175-1184.

Greenwood R.C., Barrat J.A., Scott E.R.D., Haack H., Buchanan P.C., Franchi I.A., Yamaguchi A., Johnson D., Bevan A.W.R., Burbine T.H. (2015) Geochemistry and oxygen isotope composition of main-group pallasites and olivine-rich clasts in mesosiderites: Implications for the “Great Dunite Shortage” and HED-mesosiderite connection. *Geochim. Cosmochim. Acta* **169**, 115-136.

Hanson G.N. (1980) Rare Earth Elements in petrogenetic studies of igneous systems. *Ann. Rev. Earth Planet. Sci.* **8**, 371-406.

Hewins R.H., Bourot-Denise M., Zanda B., Leroux H., Barrat J.A., Humayun M., Göpel C., Greenwood R.C., Franchi I.A., Pont S., Lorand J.P., Cornède C., Gattacceca J., Rochette P., Kuga M., Marrocchi Y., Marty B. (2014) The Paris meteorite, the least altered CM chondrite. *Geochim. Cosmochim. Acta.* **124**, 190-222.

Hiyagon H., Yamakawa A., Ushikubo T., Lin Y., Kimura M. (2011) Fractionation of rare earth elements in refractory inclusions from the Ningqiang meteorite: origin of positive anomalies in Ce, Eu and Yb. *Geochim. Cosmochim. Acta* **75**, 3358-3384.

Huang S., Farkas J., Yu G., Petaev M.I., Jacobsen S.B. (2012) Calcium isotopic ratios and rare earth element abundances in refractory inclusions from Allende CV3 chondrite. *Geochim. Cosmochim. Acta* **77**, 252-265.

Irving A.J., Kuehner S.M., Bunch T.E., Ziegler K., Chen G., Herd C.D.K., Conrey R.M., Ralew S. (2013) Ungrouped mafic achondrite Northwest Africa 7325: a reduced iron-poor cumulate olivine gabbro from a differentiated planetary parent body. *44th Lunar and Planetary Science Conference*, abstract # 2164.

Javoy M., Kaminski E., Guyot F., Andraut D., Sanloup C., Moreira M., Labrosse S., Jambon A., Agrinier P., Davaille A., Jaupart C. (2010) The chemical composition of the Earth: enstatite chondrite models. *Earth Planet. Sci. Lett.* **293**, 259-268.

Khan R., Shirai N., Ebihara M. (2015) Chemical characteristic of R chondrites in the light of P, REEs, Th and U abundances. *Earth Planet. Sci. Lett.* **422**, 18-27.

Koeberl C. (1992) Geochemistry and origin of Muong Nong –type tektites. *Geochim. Cosmochim. Acta* **56**, 1033-1064.

- Lodders K. (2000) an oxygen isotope mixing model for the accretion and composition of rocky planets. *Space Science Reviews* **92**, 341–354,
- Lodders K. (2003) Solar system abundances and condensation temperatures of the elements. *Astrophys. J.* **591**, 1220–1247.
- Magna T., Gussone N., Mezger K. (2015) The calcium isotope systematics of Mars. *Earth Planet. Sci. Lett.* **430**, 86–94.
- Masuda A. (1962) Regularities in variation of relative abundances of Lanthanide elements and an attempt to analyse separation index patterns of some minerals. *J. Earth Sci. Nagoya Univ.* **10**, 173–187.
- MacPherson G.J. (2003) Calcium-aluminum-rich inclusions in chondritic meteorites. In meteorites, Comets and Planets (ed. A. M. Davis) Vol. 1 Treatise on Geochemistry (eds. H.D. Holland and K.K. Turekian), pp. 201–246 Elsevier-Pergamon, Oxford.
- Mason B., Taylor S.R. (1982) Inclusions in the Allende meteorite. *Smithsonian Contrib. Earth Sci.* **25**, pp 1–30.
- Moynier F., Beck P., Jourdan F., Yin Q.-Z., Reimold W. U. and Koeberl C. (2009) Isotopic fractionation of zinc in tektites. *Earth Planet. Sci. Lett.* **277**, 482–489.
- Moynier F., Koeberl C., Beck P., Jourdan F., Telouk P. (2010) Isotopic fractionation of Cu in tektites. *Geochimica Cosmochimica Acta* **74**, 799–807.
- Morlok A., Bischoff A., Stephan T., Floss C., Zinner E., Jessberger E.K. (2006) Brecciation and chemical heterogeneities of CI chondrites. *Geochimica et Cosmochimica Acta* **70**, 5371–5394.
- Nance W.B., Taylor S.R., (1976) Rare earth element patterns and crustal evolution—I. Australian post-Archean sedimentary rocks. *Geochimica et Cosmochimica Acta* **40**, 1539–1551.
- Pack A., Shelley J. M. G. and Palme H. (2004) Chondrules with peculiar REE patterns: implications for nebular condensation at high C/O. *Science* **303**, 997–1000.
- Palme H., Lodders K. and Jones A. (2014) Solar System Abundances of the Elements. In: Holland H.D. and Turekian K.K. (eds.) Treatise on Geochemistry, Second Edition, vol. 2, pp. 15–36. Oxford: Elsevier.
- Pourmand, A., Dauphas, N., Ireland, T.J. (2012) A novel extraction chromatography and MC-ICP-MS technique for rapid analysis of REE, Sc and Y: Revising CI-chondrite and Post-Archean Australian Shale (PAAS) abundances. *Chem. Geol.* **291**, 38–54.
- Pourmand A., Prospero J., Sharifi M., Arash. (2014) Geochemical fingerprinting of trans-Atlantic African dust based on radiogenic Sr-Nd-Hf isotopes and rare earth element anomalies. *Geology*, doi:10.1130/g35624.1
- Raczek L., Stoll B., Hofmann A. W. and Jochum K. P. (2001) High precision trace element data for the USGS reference materials BCR-1, BCR-2, BHVO-1, BHVO-2, AGV-1, AGV-2, DTS-1, DTS-2, GSP-1 and GSP-2 by ID-TIMS and MIC SSMS. *Geostand. Newsl.* **25**, 77–86.
- Sanloup C., Jambon A., Gillet P. (1999) A simple chondritic model of Mars. *Phys. Earth Planet. Interiors* **112**, 43–54.
- Shinotsuka K., Hidaka H. and Ebihara M. (1995) Detailed abundances of rare earth elements, thorium and uranium in chondritic meteorites: an ICP-MS study. *Meteoritics* **30**, 694–699.
- Siebert J., Badro J., Antonangeli D., Ryerson F.J. (2013) Terrestrial accretion under oxidizing conditions. *Science* **339**, 1194–1197.
- Stracke A., Palme H., Gellissen M., Münker C., Kleine T., Birbaum K., Detlef G., Bourdon B., Zipfel J. (2012) Refractory element fractionation in the Allende meteorite: Implications for solar nebula condensation and the chondritic composition of planetary bodies. *Geochim. Cosmochim. Acta* **85**, 114–141.

Tanaka T., Masuda A. (1973) Rare Earth Elements in matrix, inclusions, and chondrules of the Allende meteorite. *Icarus* **19**, 523-530.

Taylor S.R., McLennan S.M. (1981) The composition and evolution of the continental crust: rare earth element evidence from sedimentary rocks. *Phil. Trans Royal Soc. London Ser. A*, **301**, 381-399.

Toplis M.J., Mizzon H., Monnereau M., Forni O., McSween H.Y., Mittlefehldt D.W., McCoy T.J., Prettyman T.H., De Sanctis M.C., Raymond C.A., Russell C.T. (2013) Chondritic models of 4 Vesta; implications for geochemical and geophysical properties. *Meteoritics Planetary Sci.* **48**, 2300-2315.

Valdes M.C., Moreira M., Foriel J., Moynier F. (2014) The nature of Earth's building blocks as revealed by calcium isotopes. *Earth Planet. Sci. Lett.*, **394**, 135-145.

Warren P.H. (2011a) Stable isotopes and the noncarbonaceous derivation of ureilites, in common with nearly all differentiated planetary materials. *Geochim. Cosmochim. Acta* **75**, 6912-6926.

Warren P.H. (2011b) Stable-isotopic anomalies and the accretionary assemblage of the Earth and Mars: A subordinate role for carbonaceous chondrites. *Earth Planet. Sci. Lett.*, **311**, 93-100.

Yamakawa A., Yamashita K., Makashima A. and Nakamura E. (2010) Chromium isotope systematics of achondrites: chronology and isotopic heterogeneity of the inner solar system. *Astrophys. J.* **720**, 150-154.

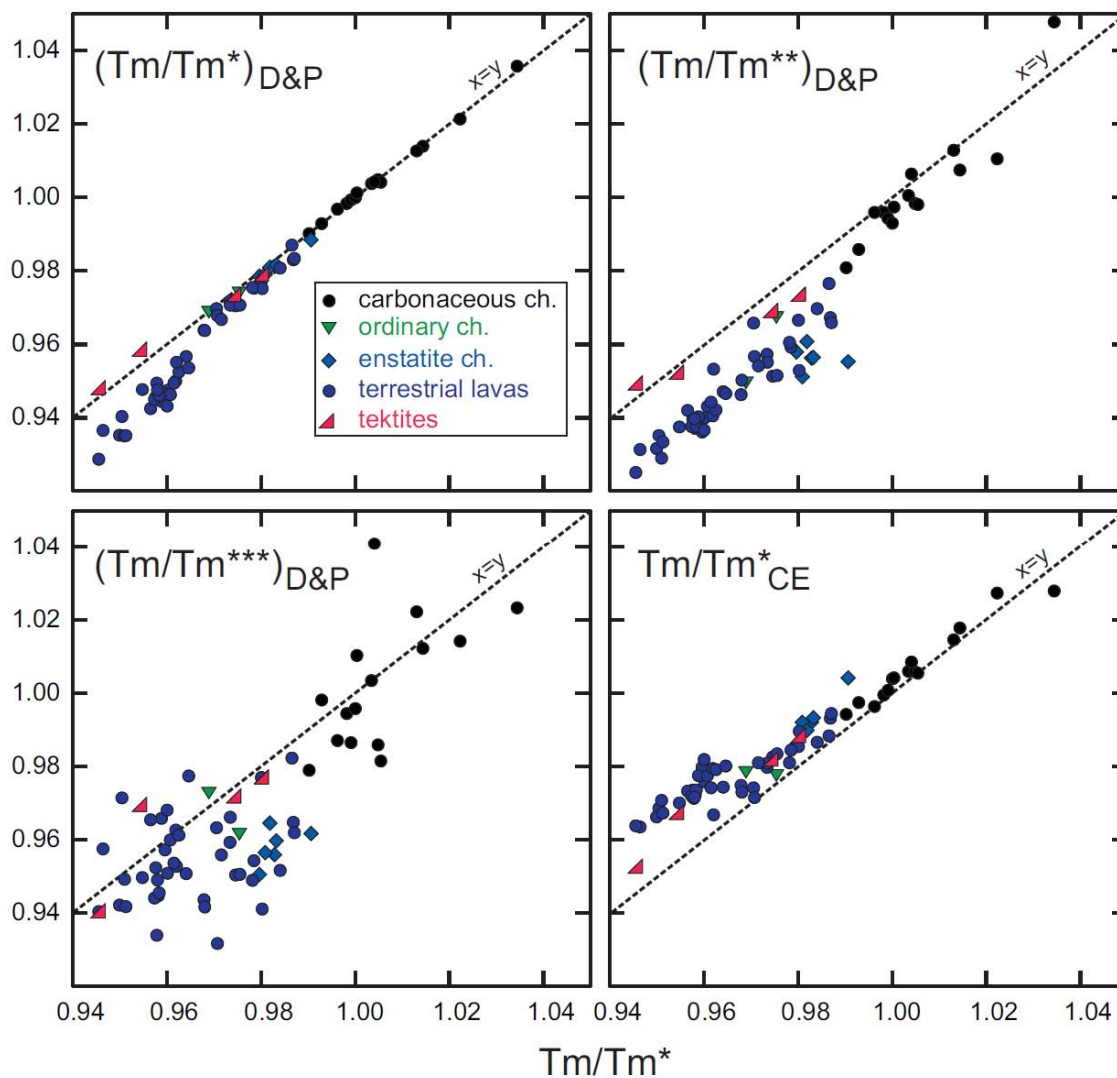


Fig. 1. Comparison of the Tm/Tm^* , Tm/Tm^{**} , Tm/Tm^{***} ratios calculated using the equations given by Dauphas and Pourmand (2015), and Tm/Tm^{*}_{CE} with the Tm/Tm^* ratios proposed in this study, for a selection of chondrites and terrestrial rocks.

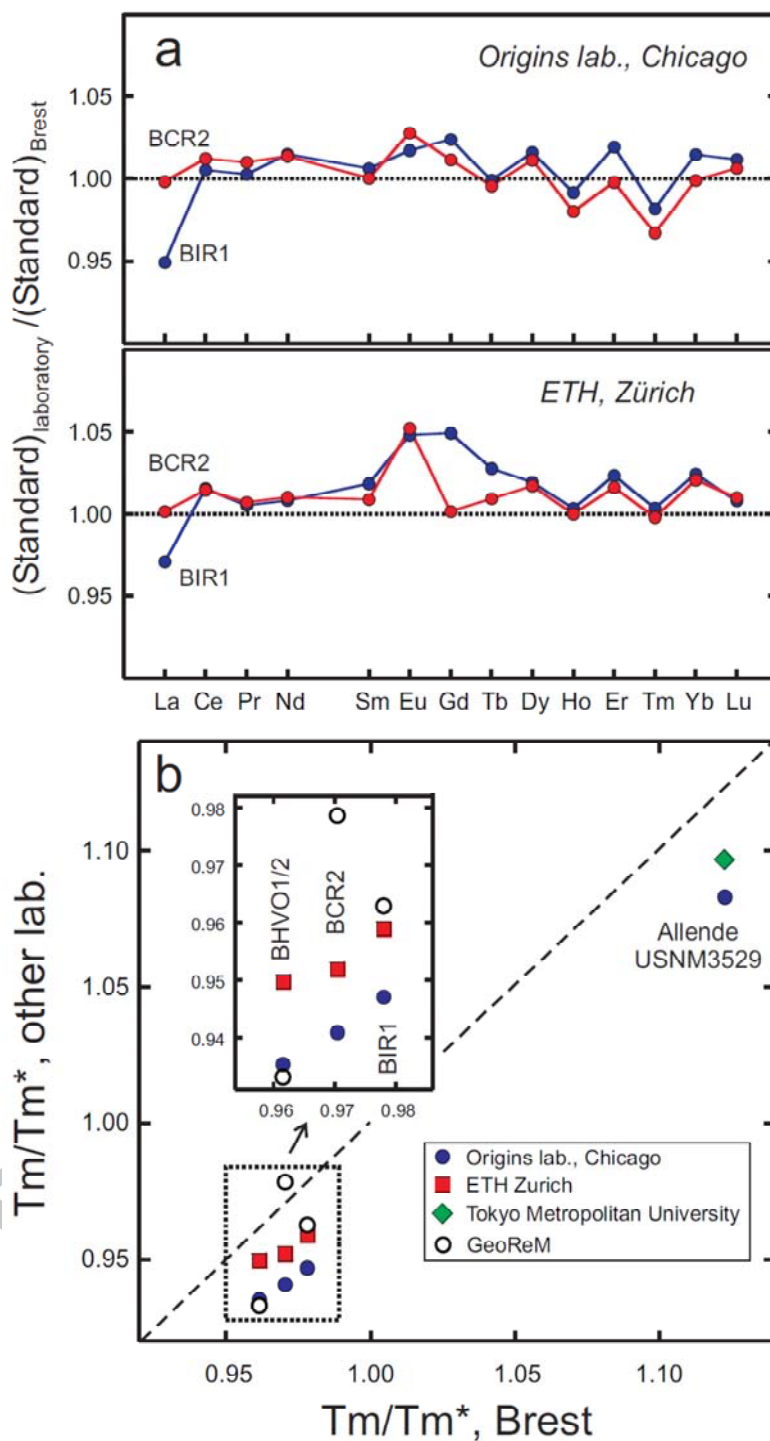


Fig. 2. Comparison of the REE abundances (a), and the Tm/Tm^* ratios for reference materials obtained during the course of this study in Brest, with those, uncorrected, obtained at ETH (Stracke et al., 2012), Origins laboratory (Pourmand et al., 2012), Tokyo Metropolitan University (Khan et al., 2015) and the GEOREM's preferred values (georem.mpch-mainz.gwdg.de). Tm/Tm^* ratios are relative to the CI data recommended by Barrat et al. (2012). Although the Tm/Tm^* values obtained in the different laboratories vary slightly, the results are highly coherent.

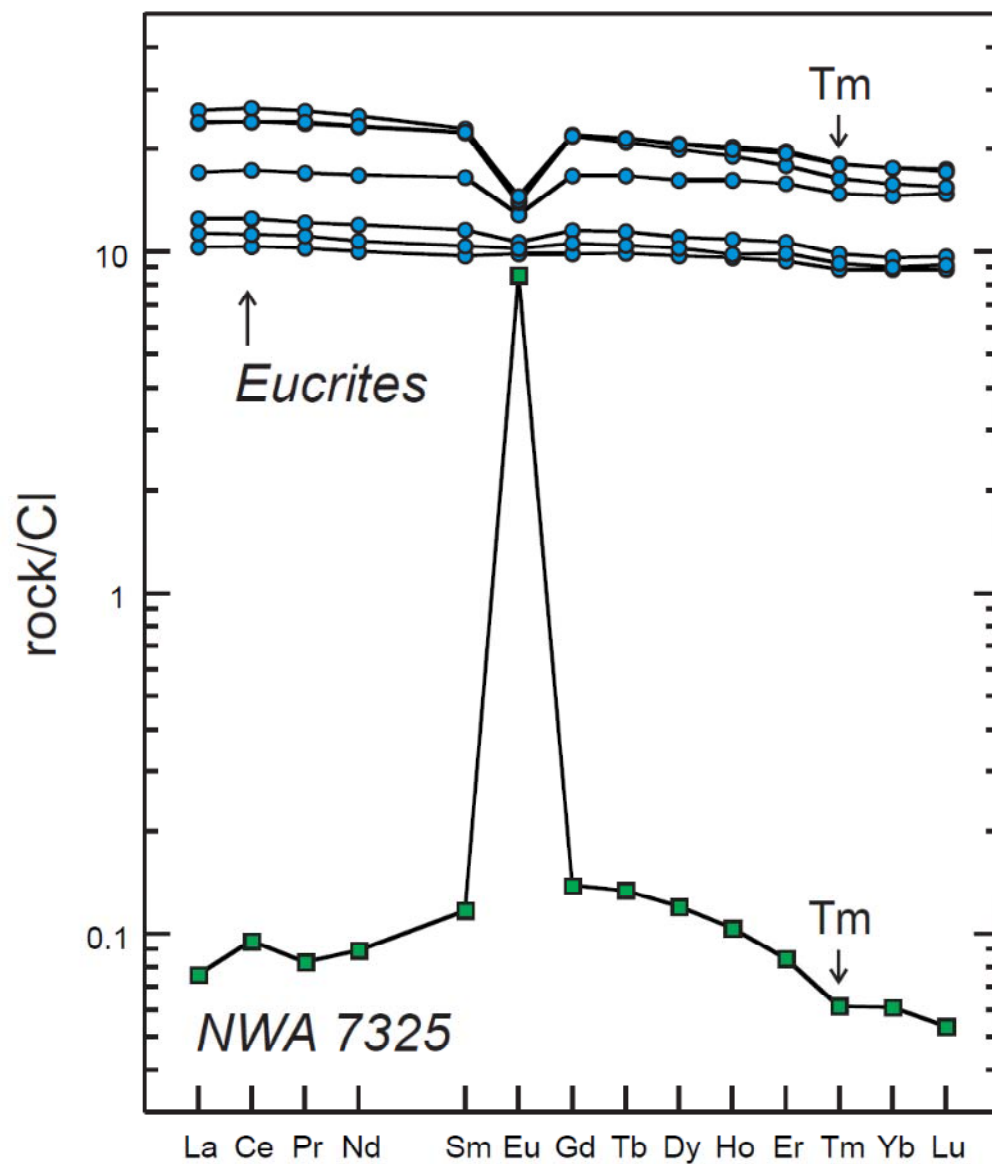


Fig. 3. REE patterns for eucrites and the ungrouped achondrite NWA 7325 normalized to CI chondrite (Barrat et al., 2012). The negative Tm anomalies are generally too small to be easily discerned on the REE patterns of achondrites or planetary samples, excepted for NWA 7325.

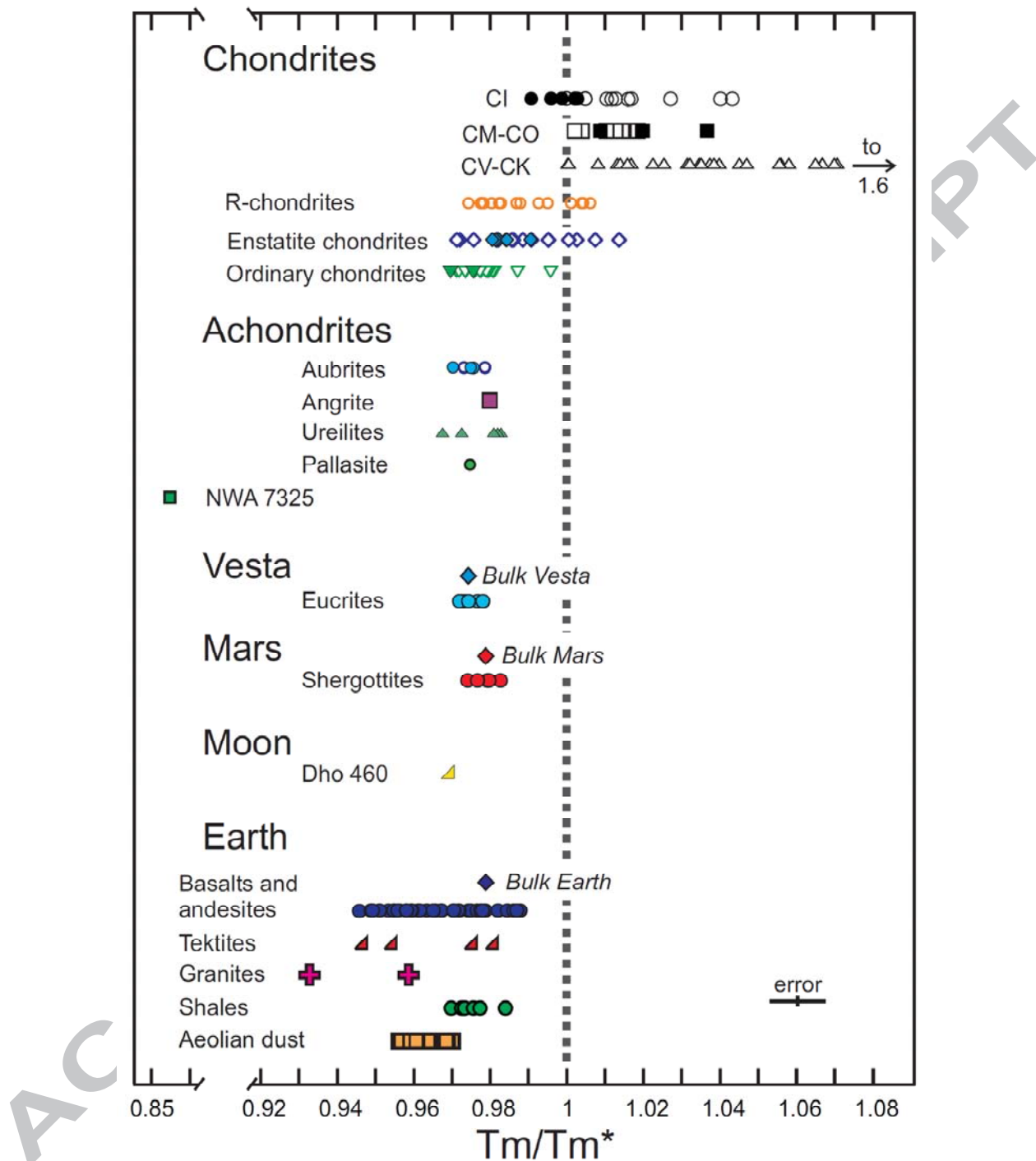


Fig. 4. T_m/T_m^* ratios relative to CI among meteorites and planetary samples (open symbols: Pourmand et al., 2012; Stracke et al., 2012; Bischoff et al., 2012; Dauphas and Pourmand, 2015; Khan et al., 2015; filled symbols: this study). Literature data are adjusted to the Brest BIR-1 and BCR-2 values and T_m/T_m^* ratios are relative to the CI data recommended by Barrat et al. (2012).

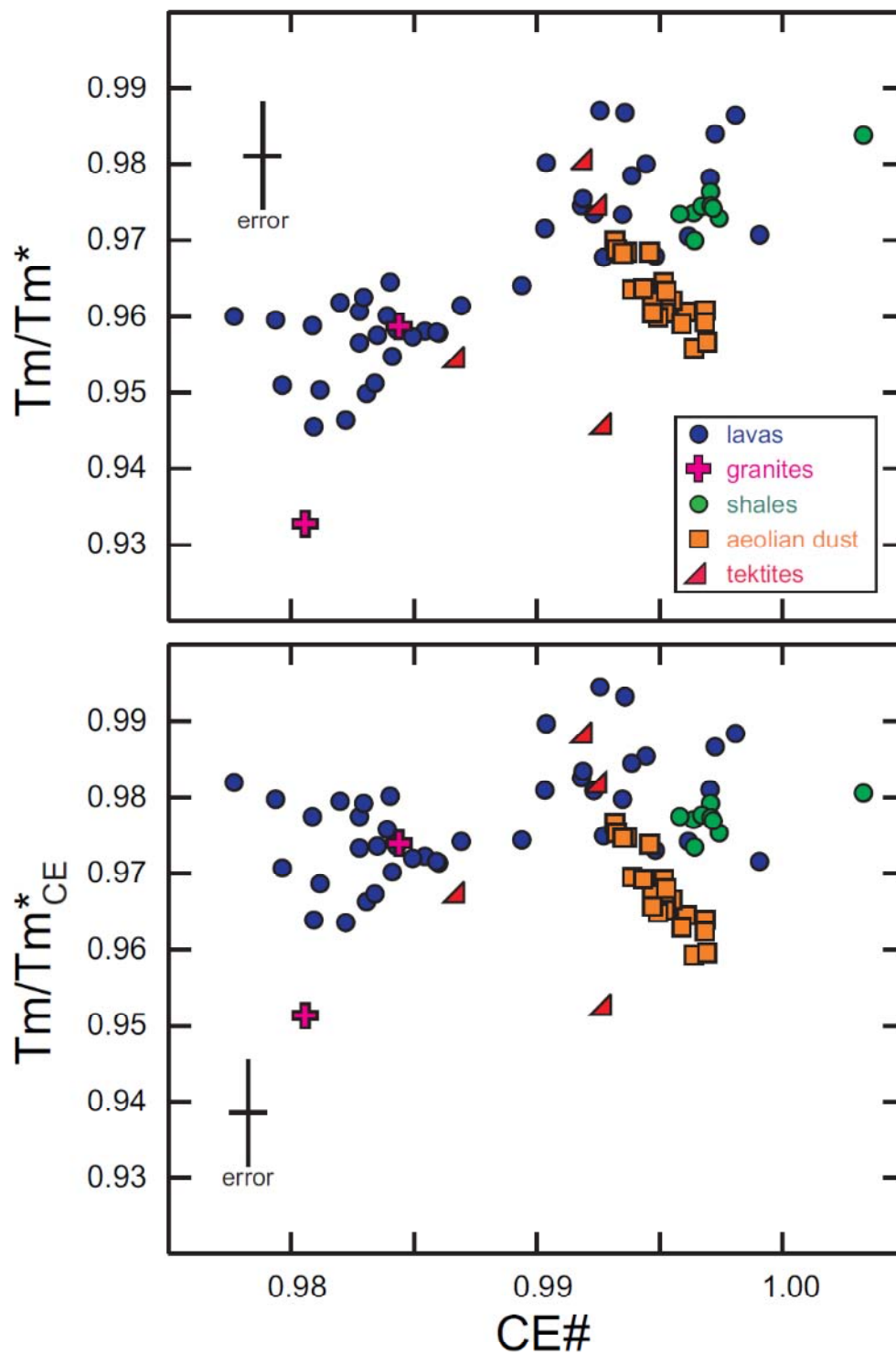


Fig. 5. Tm/Tm^* and Tm/Tm^*_{CE} vs. CE# plots for terrestrial samples (Pourmand et al., 2012, 2014; this study). Literature data are adjusted to the Brest BIR-1 and BCR-2 values and Tm/Tm^* ratios are relative to the CI data recommended by Barrat et al. (2012).

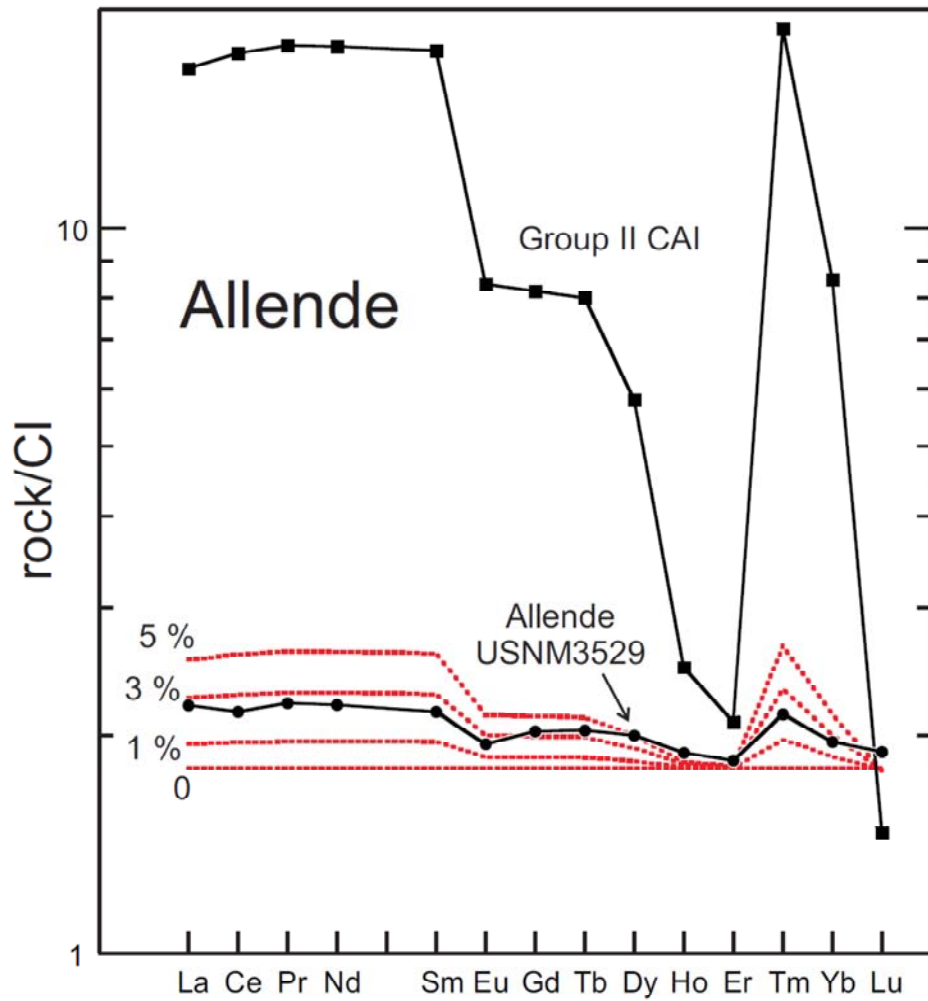


Fig. 6. REE patterns for the Allende CV chondrite (USNM3529, Barrat et al., 2012) and the mean of two group II CAIs obtained by Huang et al. (2012). The REE abundances of this chondrite can be easily reproduced by an addition of 2-3 wt% of this type of CAIs in a chondritic material with REE concentrations = 1.8 x CI abundances.

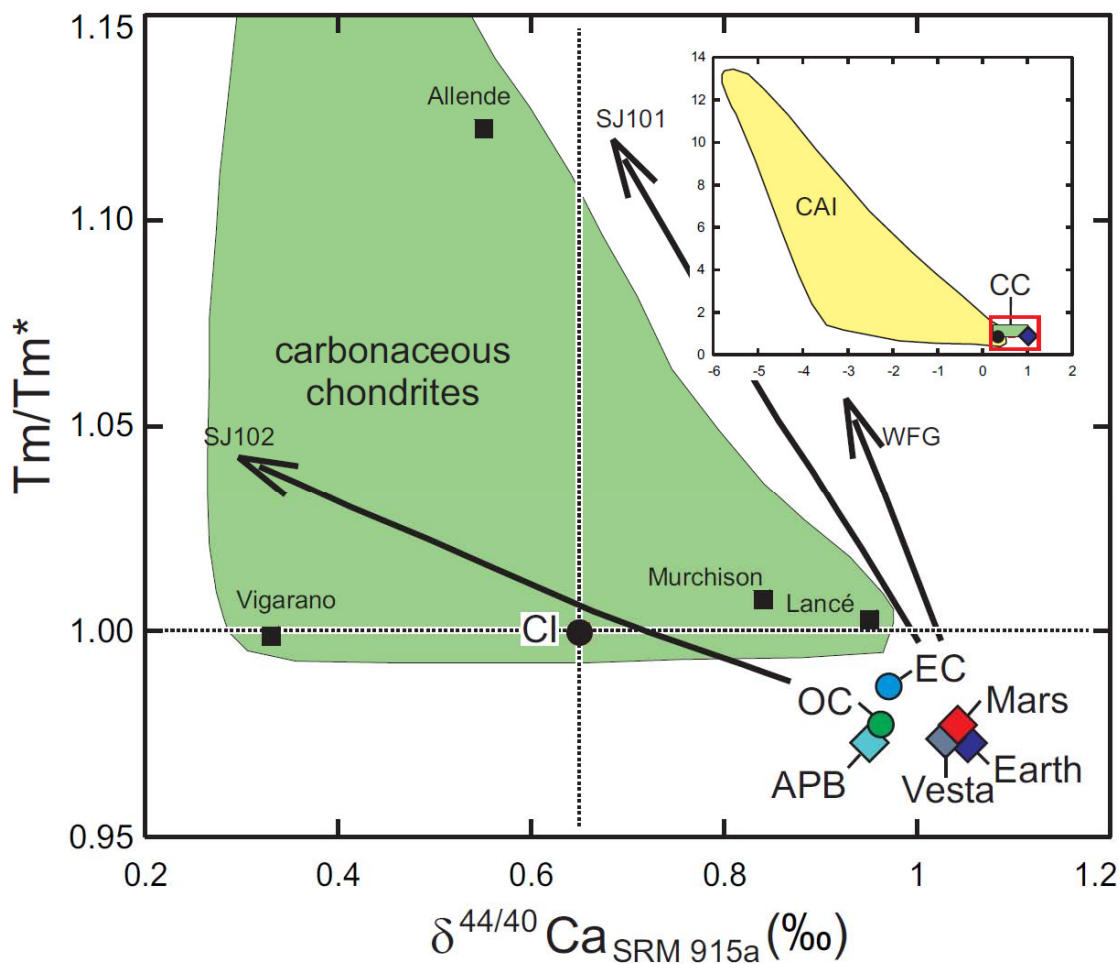


Fig. 7. Relationship between Tm/Tm^* ratios and Ca isotopic composition in chondrite groups, Earth, Mars, Vesta and the aubrite parent body (APB). The black arrows indicate mixing between a bulk silicate Earth composition and selected refractory inclusions analyzed by Huang et al. (2012). The labels on the curves correspond to the names of the inclusions used in the calculations. Tm/Tm^* values for Murchison, Lance, and Vigarano are from Dauphas and Pourmand (2015). Ca isotopic compositions are from Valdes et al. (2014) and Magna et al. (2015).

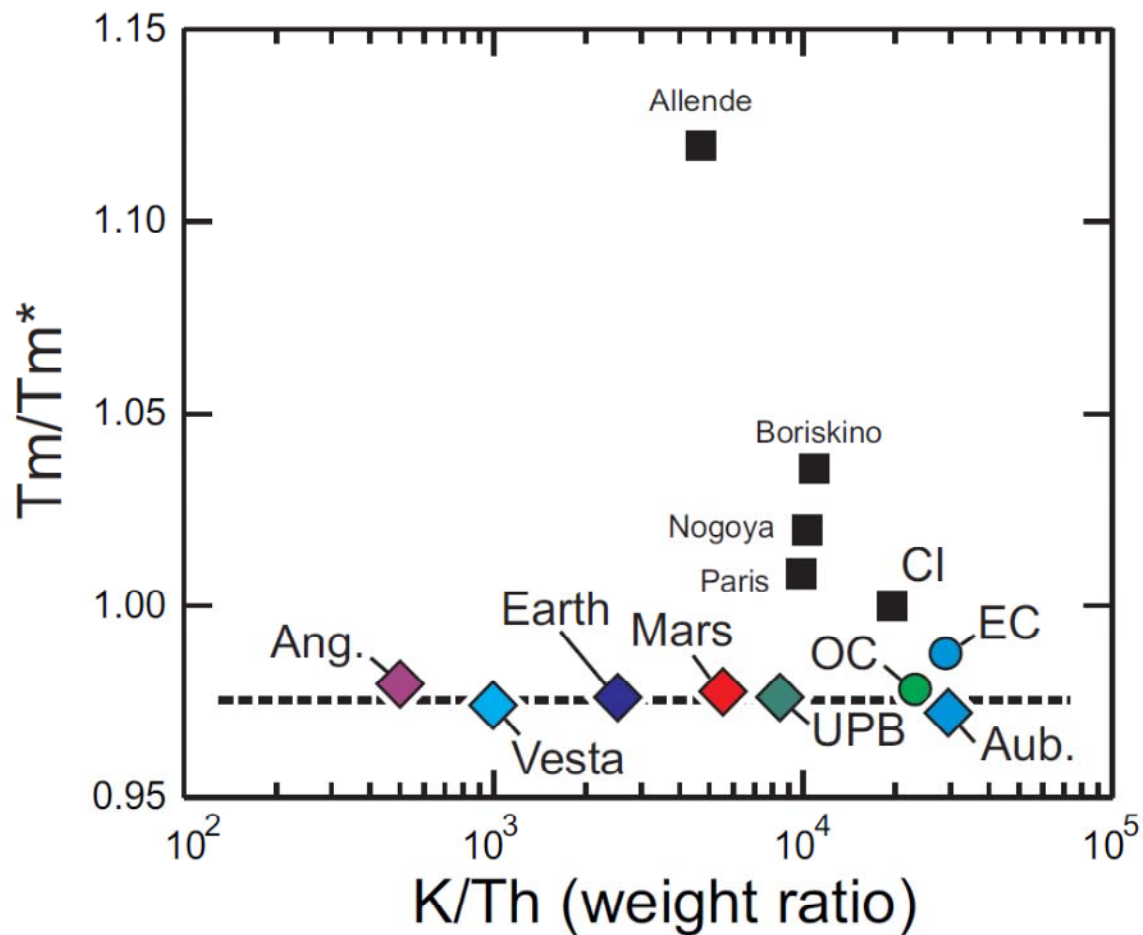


Fig. 8. Plot of T_m/T_m^* vs. K/Th ratios for bulk differentiated bodies and chondrites. The angrite parent body (Ang.) is inferred from NWA 1296, the sole angrite analyzed in this study. The aubrite parent body (Aub.) and enstatite chondrites are assumed to share the same K/Th ratio. The K/Th ratio of the ureilite parent body (UPB) is inferred from the ALMA trachyandesite (Bischoff et al., 2014). Data for carbonaceous chondrites (black squares) are from Barrat et al. (2012), Hewins et al. (2014) and this study.

Table1. REE abundances in basaltic (BHVO-2, BCR-2, BIR-1, BE-N, JB2) and andesitic (JA3) reference materials (in $\mu\text{g/g}$). A to F are replicates from different dissolutions of the same reference material.

	La	Ce	Pr	Nd	Sm	Eu	Gd	Tb	Dy	Ho	Er	Tm	Yb	Lu	Tm/Tm*	CE#
BHVO-2																
working values	15.2	37.5	5.31	24.5	6.07	2.07	6.24	0.94	5.3	1.00	2.5	0.34	2.0	0.27	0.962	0.987
BCR-2 A	25.2 8	53.3 2	6.89	28.8 2	6.51	1.86	6.63	1.05	6.3 8	1.31	3.6 3	0.52 8	3.3 4	0.48 3	0.965	0.990
BCR-2 B	25.3 9	53.4 4	6.75	28.8 8	6.58	1.90	6.67	1.04	6.4 3	1.30	3.6 3	0.53 6	3.3 6	0.47 6	0.979	0.995
BCR-2 C	24.8 1	52.9 2	6.69	28.4 1	6.55	1.91	6.77	1.06	6.3 6	1.32	3.6 5	0.52 7	3.3 4	0.48 1	0.963	0.990
BCR-2 D	24.2 8	52.6 7	6.69	28.3 2	6.52	1.93	6.75	1.05	6.3 5	1.31	3.6 7	0.53 7	3.3 6	0.49 2	0.974	0.990
BCR-2 E	24.7 2	52.3 8	6.68	28.3 5	6.52	1.93	6.72	1.05	6.3 3	1.31	3.6 6	0.53 4	3.3 7	0.48 9	0.969	0.991
BCR-2 F	24.6 5	52.1 9	6.68	28.2 0	6.46	1.94	6.72	1.05	6.3 6	1.31	3.6 8	0.53 6	3.3 6	0.49 2	0.972	0.990
BCR-2 (n=6)	24.8 6	52.8 2	6.73	28.5	6.52	1.91	6.71	1.05	6.3 7	1.31	3.6 5	0.53 3	3.3 5	0.48 6	0.97	0.991
RSD%	1.67	0.95	1.27	1.00	0.63	1.56	0.75	0.67	5	0.38	7	0.83	5	1.33	0.60	0.19
BIR-1 A	0.62 4	1.92	0.37 1	2.37	1.09	0.51 8	1.81	0.35 9	2.5 6	0.58 3	1.7 0	0.25 7	1.6 5	0.24	0.981	0.997
BIR-1 B	0.62 7	1.93	0.37 3	2.37	1.08	0.51 5	1.8	0.35 9	2.5 6	0.57 9	1.7 1	0.25 6	1.6 3	0.24 2	0.977	0.996
BIR-1 C	0.62 6	1.87	0.37 3	2.38	1.07	0.52 1	1.84	0.36 1	2.5 7	0.57 3	1.7 0	0.25 5	1.6 4	0.24 4	0.973	0.997
BIR-1 D	0.62 8	1.89	0.37 4	2.38	1.08	0.51 8	1.84	0.36 1	2.5 6	0.57 4	1.6 9	0.25 6	1.6 4	0.24 1	0.979	0.997
BIR-1 E	0.61 2	1.89	0.36 7	2.37	1.08	0.51 7	1.82	0.36 6	2.5 1	0.58 1	1.7 1	0.25 9	1.6 5	0.24 4	0.982	0.996
BIR-1 F	0.61 3	1.89	0.36 8	2.35	1.08	0.52 2	1.83	0.36 4	2.5 7	0.57 3	1.7 2	0.25 7	1.6 3	0.24 5	0.978	0.997
BIR-1 (n=6)	0.62 2	1.90	0.37 1	2.37	1.08	0.51 8	1.82	0.36 1	2.5 6	0.57 7	1.7 1	0.25 7	1.6 4	0.24 3	0.978	0.997
RSD%	1.17	1.24	0.80	0.52	0.38	0.46	0.84	0.53	3	0.74	3	0.57	4	0.8	0.29	0.06
Eu-spiked BIR-1	0.61 8	1.90	0.37	2.36	1.08	52.3 9	1.84	0.36 3	2.5 5	0.57 5	1.7 1	0.25 6	1.6 4	0.24 4	0.974	0.997
BE-N A	84.8 1	155. 4	17.0 6	65.7 7	12.0 1	3.67	7	10.1 7	6.3 9	1.09	2.5 6	0.32 0	1.8 1	0.23 5	0.949	0.980
BE-N B	84.7 7	154. 9	17.2 6	66.0 4	11.9 8	3.61	9.56	12.6 4	6.3 4	1.08	2.5 5	0.31 8	1.8 1	0.23 5	0.946	0.981
JB2	2.35	6.81	1.17	6.40	2.24	0.79 1	3.18	0.58 3	3.9 2	0.86 4	2.5 2	0.38 1	2.4 7	0.36 8	0.972	0.993
JA3	9.84	21.9	2.94	12.9 4	3.17 1	0.77	3.29	0.54 8	3.4 3	0.72 8	2.1 0	0.31 9	2.0 9	0.30 3	0.970	0.996

Table 2. REE abundances in chondrites (in $\mu\text{g/g}$). A and B correspond to duplicates of the same solutions obtained during different sessions.

	La	Ce	Pr	Nd	Sm	Eu	Gd	Tb	Dy	Ho	Er	Tm	Yb	Lu	Tm/Tm*	CE#
<i>Recommended CI,</i>																
<i>Barrat et al. (2012)</i>	0.23 5	0.6	0.091	0.46 4	0.15 3	0.058 6	0.20 6	0.037 5	0.25 4	0.056 6	0.16 6	0.026 2	0.16 8	0.024 2	1	1
Carbonaceous chondrites																
Orgueil 1 (CI)	0.24 0	0.60 0	0.090 7	0.45 0	0.14 5	0.055 4	0.19 6	0.035 9	0.23 8	0.053 2	0.15 5	0.024 3	0.15 7	0.023 1	0.991	0.99 5
Orgueil 2-A (CI)	0.25 7	0.64 1	0.098	0.48 8	0.15 8	0.061 6	0.21 3	0.039 4	0.26 2	0.057 6	0.16 9	0.026 7	0.17 2	0.025 0	0.999	0.99 9
Orgueil 2-B (CI)	0.25 7	0.64 0	0.097 1	0.48 8	0.15 6	0.060 2	0.21 6	0.039 2	0.26 5	0.058 2	0.17 0	0.027 0	0.17 3	0.025 2	1.005	0.99 7
Orgueil 3-A (CI)	0.24 1	0.60 5	0.091 5	0.45 7	0.14 8	0.055 6	0.20 3	0.036 5	0.24 5	0.053 5	0.15 8	0.025 1	0.16 6	0.023 6	1.000	0.99 8
Orgueil 3-B (CI)	0.24 0	0.60 4	0.091 1	0.45 8	0.14 6	0.056 4	0.20 1	0.036 8	0.24 5	0.053 7	0.15 8	0.024 7	0.16 7	0.023 7	0.992	0.99 6
Orgueil 4-A (CI)	0.24 9	0.62 4	0.093 8	0.47 3	0.15 3	0.058 8	0.21 0	0.038 1	0.25 8	0.056 0	0.16 5	0.026 1	0.16 9	0.024 5	0.996	1.00 0
Orgueil 4-B (CI)	0.24 6	0.61 8	0.094 9	0.46 9	0.15 3	0.058 3	0.20 8	0.038 7	0.25 9	0.056 8	0.16 6	0.026 2	0.16 8	0.024 7	1.001	0.99 6
Orgueil 5-A (CI)	0.25 0	0.62 1	0.095 3	0.47 2	0.15 2	0.059 2	0.20 9	0.037 9	0.25 8	0.057 3	0.16 7	0.026 6	0.17 2	0.025 2	1.003	0.99 6
Orgueil 5-B (CI)	0.25 0	0.62 0	0.094 6	0.47 1	0.15 3	0.058 1	0.21 0	0.038 5	0.25 9	0.056 9	0.16 9	0.026 8	0.17 1	0.025 1	1.003	0.99 9
Ivuna (CI)	0.25 3	0.63 5	0.094 6	0.47 9	0.15 5	0.058 8	0.20 9	0.038 7	0.26 0	0.057 1	0.16 9	0.026 5	0.16 7	0.024 3	1.002	1.00 0
Boriskino 1 (CM)	0.41 8	1.01	0.141	0.68 7	0.21 2	0.078 9	0.27 9	0.050 8	0.34 2	0.073 4	0.21 8	0.036 1	0.22 7	0.031 9	1.036	1.00 6
Nogoya A (CM)	0.31 8	0.78 2	0.119	0.60 6	0.19 3	0.072 6	0.26 6	0.048 6	0.32 4	0.071 9	0.21 0	0.033 5	0.21 1	0.030 9	1.016	0.99 7
Nogoya B (CM)	0.31 6	0.77 7	0.12	0.60 1	0.19 3	0.072 8	0.26 8	0.048 6	0.32 5	0.071 9	0.21 0	0.033 6	0.20 9	0.030 9	1.023	0.99 5
Paris A (CM)	0.33 9	0.84 8	0.129	0.64 7	0.20 6	0.078 9	0.28 3	0.052 1	0.35 0	0.078 8	0.22 4	0.035 6	0.22 8	0.032 7	1.006	0.99 6
Paris B (CM)	0.33 9	0.84 7	0.128	0.64 5	0.20 7	0.079 2	0.28 3	0.052 4	0.35 0	0.078 0	0.22 6	0.036 0	0.22 7	0.032 6	1.011	0.99 8
Ordinary chondrites																
Chelyabinsk (LL)	0.33 6	0.84 9	0.127	0.62 9	0.20 0	0.067 6	0.28 1	0.050 7	0.33 7	0.074 2	0.21 7	0.032 9	0.21 3	0.031 0	0.975	0.99 8
Braunschweig (L)	0.35 1	0.91 2	0.134	0.66 2	0.21 6	0.077 5	0.30 2	0.056	0.36 6	0.084 3	0.24 7	0.037 7	0.24 9	0.038 0	0.969	0.99 0
Enstatite chondrites																
EET 87746 (EH4)	0.22 2	0.59 3	0.086 3	0.43 4	0.14 1	0.053 9	0.19 6	0.035 9	0.24 5	0.054 7	0.16 3	0.024 9	0.16 1	0.024 5	0.980	0.99 4
EET96135 (EH4/5)	0.24 7	0.65 8	0.095 5	0.48 2	0.15 6	0.058 1	0.21 7	0.040 2	0.27 4	0.061 2	0.18 1	0.027 6	0.17 7	0.027 2	0.983	0.99 1
Abee (EH5)	0.26 0	0.70 5	0.102	0.50 8	0.16 1	0.056 3	0.22 7	0.041 8	0.28 5	0.064 1	0.18 9	0.028 7	0.18 4	0.028 5	0.980	0.98 9
MAC 02747 (EL4)	0.26 6	0.69 8	0.102	0.51 5	0.16 7	0.064 7	0.22 9	0.042 2	0.29 0	0.065	0.19 2	0.029 5	0.19 1	0.029 1	0.981	0.99 2
NWA 4780 (EL4)	0.30 7	0.80 8	0.118	0.59 1	0.19 3	0.069 2	0.26 2	0.049 5	0.33 5	0.075	0.22 1	0.033 8	0.21 4	0.033 6	0.989	0.98 7
NWA 3134 (EL6)	0.29 2	0.97 5	0.156	0.80 4	0.26 5	0.043 2	0.36 5	0.067 3	0.46 1	0.102 9	0.30 3	0.046 2	0.29 6	0.045 5	0.983	0.99 0

Table 3. REE abundances in achondrites (in $\mu\text{g/g}$ or in ng/g for aubrites, ureilites, Brenham and NWA 7325). A and B correspond to duplicates of the same solutions obtained during different sessions.

	La	Ce	Pr	Nd	Sm	Eu	Gd	Tb	Dy	Ho	Er	Tm	Yb	Lu	Tm/Tm*	CE#
Angrite																
NWA 1296 A	4.82	12.1 0	1.82	8.99	2.82	1.08	3.84	0.69 7	4.6 8	1.04	3.01	0.44 6	2.79	0.41 9	0.982	0.99 1
NWA 1296 B	4.74	12.0 1	1.80	9.00	2.86	1.08	3.87	0.70 0	4.6 6	1.03	2.99	0.45 1	2.86	0.41 3	0.983	0.99 8
NWA 1296 C	4.73	11.9 6	1.79	8.95	2.85	1.09	3.9	0.70 4	4.6 8	1.03	2.99	0.44 7	2.86	0.41 5	0.974	0.99 7
Aubrites (in ng/g)																
LAR 04316	169	552	95.2	517	178	31.1	256	46.6	313	68.3	197	28.8	180	26.1	0.973	0.99 6
Norton County	358	1140	200	1040	329	36.9	442	77.4	502	108	311	45.0	280	41.0	0.973	0.99 4
Pena Blanca Spr.	170	466	67.3	348	128	28.7	190	34.5	229	50.2	143	21.2	136	19.7	0.969	0.99 4
Ureilites (in ng/g)																
ALH 82130	8.3	33.6	7.3	53.4	31.9	3.97	66.7	14.7	115	29.1	94.4	16.0	115	19.3	0.979	0.99 1
EET 83225.	1.3	4.9	1.6	19.5	21.5	1.71	58.8	13.8	111	28.2	91.1	15.0	108	18.1	0.964	0.99 1
MET 01085	8.3	33	6.9	52.6	34.9	6.48	84.3	20.6	175	46.3	15.9	27.7	203	33.7	0.981	1.00 3
Y-791538	1.4	5.5	1.3	11.6	11.6	1.46	34.2	8.8	77. 8	21.2	75.0	13.5	101	17.7	0.983	0.99 9
Ungrouped (ng/g)																
NWA 7325	17.9	57.2	7.50	41.5	17.9	500	28.6	5.01	30. 5	5.88	14.0	1.60	10.2	1.32	0.855	0.98 3
Pallasite (in ng/g)																
Brenham olivine	51.4	91.6	11.2	38.3	6.5	1.29	6.09	0.96 2	6.0 3	1.3	3.9	0.64 8	4.6	0.78 2	0.975	0.97 6
Eucrites																
Bereba	2.66	6.73	1.01	4.98	1.59	0.59 6	2.18	0.39 1	2.6 0	0.55 5	1.64	0.24 2	1.51	0.22 5	0.978	0.99 6
Bouvante A	5.66	14.4 5	2.19	10.8 9	3.43	0.85	4.50	0.80 2	5.2 3	1.13	3.21	0.47 1	2.97	0.42 3	0.973	0.99 7
Bouvante B	5.64	14.4 2	2.19	10.8 8	3.44	0.85 3	4.52	0.80 6	5.2 4	1.13	3.23	0.47 2	2.94	0.42	0.976	0.99 7
Juvinas	2.93	7.48	1.11	5.56	1.77	0.62 4	2.37	0.42 9	2.8 0	0.61 4	1.77	0.25 8	1.61	0.23 8	0.972	0.99 3
NWA 049	2.42	6.21	0.93	4.64	1.48	0.57 7	2.03	0.37 1	2.4 7	0.54 3	1.56	0.23 2	1.49	0.21 8	0.972	0.99 4
NWA 2061	6.12	15.8 7	2.36	11.6	3.51	0.82 9	4.48	0.78 3	5.0 6	1.08	2.96	0.42 9	2.65	0.38 1	0.977	0.98 9
Nuevo Laredo	4.01	10.4	1.55	7.77	2.52	0.75 0	3.43	0.62 5	4.1 1	0.91 5	2.63	0.38 7	2.45	0.36 4	0.973	0.99 2
Stannern	5.61	14.4 6	2.16	10.8	3.40	0.81 7	4.53	0.80 7	5.2 8	1.15	3.26	0.47 3	2.95	0.42 9	0.973	0.99 3
Shergottites																
DAG 476	0.12 4	0.31 4	0.06 3	0.45 6	0.37	0.19 4	0.88 9	0.19 2	1.3 7	0.30 6	0.87 4	0.13 0	0.81 1	0.11 9	0.983	0.99 3
EETA79001litho. A	0.36 3	0.87	0.14 6	0.95 3	0.66 8	0.36 8	1.36	0.28 1	1.9 5	0.41 6	1.17	0.16 6	1.04	0.14 6	0.974	0.99 7
Los Angeles	2.36	5.73	0.81 5	4.13	1.65	0.87 4	2.67	0.51 3	3.4 5	0.74	2.06	0.29 8	1.85	0.26 1	0.970	0.99 5
NWA 1950	0.61	1.54	0.23 5	1.35	0.74 5	0.34 1	1.39	0.26 9	1.7 6	0.36 6	0.98 4	0.13 8	0.81 5	0.11 3	0.979	0.99 2
NWA 1669 A	1.95	4.77	0.70 0	3.54	1.40	0.56 0	2.24	0.42 7	2.8 6	0.60 1	1.67	0.24 0	1.45	0.20 4	0.981	0.99 5
NWA 1669 B	1.92	4.64	0.67 4	3.40	1.35	0.55 8	2.23	0.43 0	2.8 5	0.60 6	1.68	0.24 5	1.52	0.21 6	0.977	0.99 3

Tissint	0.30 1	0.93	0.19 3	1.37	0.86 3	0.41 0	1.67	0.32 9	2.2 5	0.46 8	1.31	0.18 9	1.16	0.16 3	0.980	0.99 6
Lunar meteorite																
Dhofar 460 A	2.41	6.37	0.81 9	3.75	1.05	0.74 5	1.28	0.23	1.4 9	0.32 3	0.91 9	0.13 5	0.85 9	0.12 1	0.969	0.99 9
Dhofar 460 B	2.42	6.35	0.82 2	3.71	1.05	0.74 5	1.28	0.22 8	1.4 9	0.32	0.91 9	0.13 5	0.86 6	0.12 2	0.968	1.00 0

Table 4. REE abundances in terrestrial lavas, indochinites and Libyan Desert Glasses (in $\mu\text{g/g}$). A, B correspond to duplicates of the same solution analyzed during different sessions.

	La	Ce	Pr	Nd	Sm	Eu	Gd	Tb	Dy	Ho	Er	Tm	Yb	Lu	Tm/Tm*	CE#	
Mid Atlantic Ridge																	
MAPCO/CH98 DR11	2.75	9.18	1.65	9.42	3.44	1.26	4.85	0.90 6	6.02	1.32	3.81	0.571	3.57	0.526	0.986	0.99 4	
FAMOUS/CH31- DR2	7.55	17.0 6	2.40	11.3 1	3.30	1.14	4.26	0.75 7	4.98	1.09	3.14	0.463	2.92	0.434	0.974	0.99 2	
FAMOUS/CH31- DR5	4.41	10.4 2	1.46	7.07	2.18	0.81	2.93	0.53	3.5	0.76 6	2.21	0.324	2.06	0.305	0.966	0.99 3	
A127 299 DR55	2.85	7.58	1.19	6.34	2.19	0.83 5	3.15	0.58 8	3.98	0.89 1	2.57	0.384	2.46	0.365	0.975	0.99 2	
E Pacific Ridge																	
SEARISE/SR1 DR04	5.14	15.3 2	2.62	14.0 7	4.76	1.68	6.45	1.16	7.66	1.66	4.79	0.719	4.50	0.667	0.988	0.99 3	
E Rift, Easter plate																	
PI 18-06	0.50 4	2.13	0.46 4	3.00	1.30	0.58 2	2.18	0.43 2	3.16	0.74 3	2.23	0.349	2.28	0.34	0.987	0.99 8	
PI 19-02	1.46	5.20	0.97 0	5.65	2.17	0.84 2	3.20	0.59 2	3.94	0.88 3	2.54	0.382	2.43	0.355	0.978	0.99 4	
PI 19-09	4.67	12.7 7	2.00	10.5 6	3.57	1.27	4.81	0.87 1	5.57	1.22	3.50	0.513	3.21	0.475	0.977	0.99 2	
Pacific-Antarctic Ridge																	
PC1/DR03-1	5.59	15.3 0	2.42	12.4 5	3.99	1.46	5.28	0.94 4	6.14	1.33	3.83	0.56	3.55	0.518	0.967	0.99 5	
Tadjoura Gulf																	
CY84/103-1	5.73	13.6 2	1.99	9.74	3.04	1.11	4.09	0.73 3	4.88	1.07	3.11	0.465	2.95	0.437	0.979	0.99 4	
A3D3	1.93	5.06	0.80 5	4.34	1.54	0.63 5	2.31	0.42 9	2.99	0.65 2	1.93	0.287	1.84	0.269	0.972	0.99 9	
E Indian Ridge																	
HYAMS/DR3-10	41.6 4	88.4 0	11.2 2	43.9 7	10.9 1	3.09	11.8 5	1.96	12.0 7	2.54	7.28	1.07	6.65	0.992	0.982	0.99 0	
HYAMS/DR9-7	4.01	11.6 4	1.96	10.4 1	3.51	1.3	4.84	0.86 9	5.75	1.24	3.62	0.544	3.43	0.500	0.984	0.99 7	
French Massif Central																	
Gergovie	50.3 0	90.2 8	10.1 9	38.6 9		7.37	2.32	6.46	0.90 8	4.89	6	2.25	0.303	1.84	0.251	0.950	0.98 1
Cantal, IC3	125. 6	201. 3	20.3 9	69.3 4	10.6 7	3.07	8.31	1.13	5.89	1.08	2.84	0.393	2.41	0.339	0.958	0.98 6	
Cantal, IC6	26.8 1	52.3 7	6.22 2	25.4 5.54	1.80	5.41	5.41	0.78 8	4.32	4	2.09	0.280	1.66	0.229	0.958	0.98 5	
Cantal, IC11	105. 4	186. 6	20.3 0	72.5 2	12.2 3	3.60	9.90	1.33	6.99	1.28	3.20	0.431	2.63	0.360	0.946	0.98 2	
Cantal, SC2	71.1 4	134. 8	15.4 2	58.7 8	10.6 5	3.26	9.03	1.23	6.48	1.17	2.91	0.388	2.29	0.310	0.958	0.98 4	
Cantal, SC4	24.8 8	51.4 6	6.44 6	26.7 6	5.93	1.89	5.61	0.80 8	4.44	8	2.02	0.269	1.57	0.213	0.960	0.98 4	
Cantal, SC5	59.0 0	112. 2	13.1 5	51.0 2	9.54	2.89	8.13	1.09	5.75	1.02	2.49	0.329	1.92	0.261	0.960	0.97 9	
Tubuai (Austral Islands, French Polynesia)																	
TB1	60.4 1	115. 4	13.1 9	50.2 6		9.18	2.83	7.95	1.09	5.71	1.01	2.42	0.315	1.81	0.239	0.959	0.98 1
TB24	70.5 1	138. 4	15.9 9	61.4 9	11.3 0	3.45	9.73	1.33	7.00	1.24	3.00	0.391	2.24	0.296	0.961	0.98 3	
TB60	136. 2	243. 6	26.2 5	92.4 1	15.2 7	4.53	12.3 3	1.66	8.61	1.50	3.64	0.468	2.70	0.356	0.950	0.98 3	
TB113	132. 6	237. 9	25.6 0	89.7 7	14.8 6	4.45	11.9 5	1.62	8.44	1.49	3.59	0.468	2.71	0.355	0.957	0.98 3	
TB131	75.6 6	144. 9	16.6 2	62.7 1	11.6 1	3.53	9.97	1.35	7.00	1.21	2.86	0.362	2.06	0.272	0.951	0.98 0	

TB140	113.3	212.0	23.75	86.52	14.83	4.41	6	1.64	8.52	1.46	3.49	0.442	2.51	0.325	0.951	0.983
TB207	50.7	98.6	11.5	44.6	8.51	2.65	7.61	1.07	5.82	1.06	2.68	0.356	2.09	0.284	0.957	0.985
TB220	41.1	80.5	7	37.5	7.28	2.26	6.47	1	4.91	9	2.27	0.305	1.79	0.246	0.962	0.982
TB228	42.4	83.6	9	38.9	7.50	2.33	6.73	1	5.14	9	2.37	0.314	1.85	0.251	0.958	0.984
TB237	43.2	84.3	0	38.6	7.43	2.31	6.60	9	5.14	5	2.46	0.337	2.02	0.281	0.963	0.983
TB244	38.5	79.4	9	38.0	7.58	2.36	6.94	9	5.48	1.03	2.66	0.360	2.16	0.297	0.958	0.986
Other basalts																
Kaiserstuhl, KS3	56.4	102.5	11.5	43.8	7.97	2.41	6.57	0	4.30	3	1.73	0.220	1.23	0.161	0.960	0.978
Jan Mayen, JM47	92.6	178.6	20.3	74.4	12.2	3.64	9.59	1.33	7.24	1.36	3.56	0.498	3.10	0.440	0.955	0.984
Erta Ale, ER13 A	20.8	41.6	5.25	21.8	4.78	1.59	4.92	0.74	4.56	0.90	2.43	0.341	2.10	0.298	0.963	0.989
Erta Ale, ER13 B	20.3	41.3	5.17	21.7	4.82	1.61	4.91	0.76	4.48	0.90	2.43	0.344	2.12	0.298	0.967	0.990
Réunion, Chisny	21.9	46.0	6.01	26.1	6.05	2.01	6.12	0.93	5.22	1.01	2.55	0.346	2.05	0.28	0.965	0.984
Svalbard, WF27	14.4	29.6	3.71	15.5	3.66	1.17	3.99	0.65	3.91	0.80	2.20	0.311	1.93	0.267	0.961	0.995
Indochinites																
Muong Nong, Thailand	44.3	83.7	9.38	35.1	6.8	1.26	5.95	0.91	5.42	1.10	3.10	0.471	3.06	0.443	0.975	0.993
Splash form, China	42.8	82.8	9.03	34.4	6.74	1.32	6.11	0.93	5.52	1.12	3.15	0.480	3.09	0.448	0.981	0.992
Libyan Desert glasses																
LDG 7	8.78	18.9	1.95	6.97	1.24	0.21	0.97	0.14	0.78	0.15	0.43	0.067	0.47	0.071	0.954	0.987
LDG 10	6.25	13.4	1.40	5.05	0.91	0.17	0.72	0.10	0.59	0.11	0.32	0.049	0.34	0.049	0.947	0.993

Table 5. T_m/T_m^* ratios in various types of chondrites and in differentiated bodies (only bodies for which at least five samples were analyzed, are considered here). Literature data are adjusted to the Brest BIR-1 and BCR-2 values, and T_m/T_m^* ratios are relative to the CI recommended by Barrat et al. (2012).

	n	minimum	maximum	mean	σ	References
Carbonaceous chondrites						
CI	6	0.991	1.003	0.999	0.005	This work
CI	7	0.999	1.043	1.015	0.014	Dauphas and Pourmand (2015)
CM	4	1.003	1.019	1.012	0.007	Dauphas and Pourmand (2015)
CM	5	1.006	1.036	1.018	0.012	This work
CM	9	1.003	1.036	1.015	0.010	Dauphas and Pourmand (2015), this work
CV	45	1.000	1.602	1.096	0.112	Stracke et al. (2012), Dauphas and Pourmand (2015)
Other chondrites						
Enstatite chondrites	6	0.980	0.989	0.983	0.003	This work
Enstatite chondrites	16	0.971	1.013	0.989	0.012	Dauphas and Pourmand (2015)
Enstatite chondrites	22	0.971	1.013	0.987	0.011	Dauphas and Pourmand (2015), this work
Ordinary chondrites	2	0.969	0.975	0.972		This work
Ordinary chondrites	20	0.971	0.995	0.978	0.006	Dauphas and Pourmand (2015)
Ordinary chondrites	22	0.969	0.995	0.977	0.006	Dauphas and Pourmand (2015), this work
R-chondrites	15	0.975	1.007	0.989	0.011	Khan et al. (2015)

Differentiated bodies

Aubrite parent body	5	0.969	0.979	0.973	0.003	Dauphas and Pourmand (2015), this work
Ureilite parent body	5	0.964	0.983	0.976	0.008	Bischoff et al. (2014), this work
Vesta (eucrites)	7	0.972	0.978	0.974	0.002	This work
Mars (Shergottites)	6	0.970	0.983	0.977	0.005	This work

Earth

Bulk Earth (selected lavas)	18	0.962	0.987	0.976	0.007	This work
Basalts and andesites	42	0.946	0.987	0.965	0.011	This work
Post-archean shales	9	0.969	0.983	0.974	0.004	Pourmand et al. (2012)
Aeolian dust	25	0.956	0.970	0.963	0.004	Pourmand et al. (2014)

ACCEPTED MANUSCRIPT

Supplementary Table 1. Details of meteorite samples studied (IOM: Institute of Meteoritics, Albuquerque; MPI: Max Planck Institute, Mainz; MNHN : Muséum National d'Histoire Naturelle (Paris) ; MWG : Meteorite Working Group, NASA; NHM: National History Museum, Wien).

	type	source	homogenized mass (g)	dissolved mass (g)
Chondrites				
Orgueil 1	CI	MNHN, Paris	1	0.025
Orgueil 2	CI	MNHN, Paris	0.62	0.027
Orgueil 3	CI	MNHN, Paris	0.61	0.032
Orgueil 4	CI	MNHN, Paris	0.84	0.031
Orgueil 5	CI	MNHN, Paris	0.96	0.028
Ivuna	CI	MNHN, Paris	0.71	0.034
Boriskino 1	CM2	MNHN, Paris	0.5	0.124
Nogoya	CM2	MNHN, Paris	0.5	0.092
Paris	CM2	MNHN, Paris	13	0.153
Chelyabinsk	LL5	F. Paulsen	2	0.124
Braunschweig	L6	U. Münster	0.35	0.119
EET 87746	EH4	MWG	1	0.224
EET 96135	EH4/5	MWG	1	0.221
Abee	EH5	MNHN, Paris	1	0.133
MAC 02747	EL4	MWG	1	0.159
NWA 4780	EL4	MNHN, Paris	1	0.106
NWA 3134	EL6	J.A. Barrat	2	0.173
Achondrites				
Bereba	euclite (main group)	MNHN, Paris	2.1	0.102
Bouvante	euclite (Stannern)	MNHN, Paris	1.5	0.105
Juvinas	euclite (main group)	MNHN, Paris	2.8	0.098
NWA 049	euclite (main group)	ENS, Lyon	1.5	0.107
NWA 2061	euclite (unbr., Stannern)	NAU, Flagstaff	0.5	0.122
Nuevo Laredo	euclite (Nuevo Laredo)	Smithsonian Inst.	1	0.115
Stannern	euclite (Stannern)	NHM, Wien	1	0.101
DAG 476	shergottite	MPI, Mainz	5	0.138
EETA 79001litho.A	shergottite	MWG	1	0.162
Los Angeles	shergottite	B. & C. Fectay	0.04	0.040
NWA 1950	shergottite	ENS, Lyon	0.326	0.123
NWA 1669	shergottite	B. & C. Fectay	0.5	0.142
Tissint	shergottite	U Paris VI	0.5	0.109
Dhofar 460	lunar meteorite	L. Labenne, Paris	0.15	0.150
NWA 1296	angrite	U. Paris VI	0.12	0.120
LAR 04316	aubrite	MWG	2	0.153
Norton County	aubrite	IOM, Albuquerque	5	0.122
Pena Blanca Spr.	aubrite	IOM, Albuquerque	3.5	0.157
ALH 82130	ureilite	MWG	0.84	0.204
EET 83225.	ureilite	MWG	0.81	0.202
MET 01085	ureilite	MWG	0.71	0.179
Y-791538	ureilite	NIPR, Tokyo	0.5	0.184
NWA 7325	ungrouped achondrite	S. Ralew	0.6	0.102
Brenham olivine	main group pallasite	D. Stimpson	1	0.152